



**UCGE Reports  
Number 20042**

**Quality Control for Differential  
Kinematic GPS Positioning**

(URL: <http://www.geomatics.ucalgary.ca/links/GradTheses.html>)

**Department of Geomatics Engineering**

**By**

**Gang Lu**

**August 1991**



**Calgary, Alberta, Canada**

THE UNIVERSITY OF CALGARY

**QUALITY CONTROL FOR DIFFERENTIAL  
KINEMATIC GPS POSITIONING**

BY

GANG LU

A THESIS

SUBMITTED TO THE FACULTY OF GRADUATE STUDIES  
IN PARTIAL FULFILMENT OF THE REQUIREMENTS FOR THE  
DEGREE OF MASTER OF SCIENCE IN ENGINEERING

DEPARTMENT OF SURVEYING ENGINEERING

CALGARY, ALBERTA

AUGUST, 1991

© GANG LU 1991

## ABSTRACT

Kinematic differential GPS positioning is used to achieve accurate, real-time positions and velocities of a moving platform on land, in the air and at sea. In a dynamic environment, however, the deviations or biases from the assumed system and observation models are often significant. This results in a degradation of the accuracy and reliability of the estimated positions and velocities. Therefore, quality control methods are inevitably needed in a real-time positioning system to insure the system is functioning properly. In this thesis, the statistical quality control methods for use in kinematic GPS positioning are investigated. The general recursive formulas for bias influence analysis and reliability analysis in Kalman filtering are derived and the bias influence characteristics and the minimum detectable bias (MDB) values of some typical biases in differential kinematic GPS positioning are studied. A real-time statistical testing and implementation procedure for use in kinematic GPS positioning is given based on the state space two-stage Kalman filtering technique, hypothesis testing theory and reliability analysis. This procedure is for the detection of common biases such as cycle slips in carrier phases and outliers in phase rates and pseudoranges, and for the elimination of their influences on the kinematic GPS positioning results. All the derived formulas and algorithms were implemented in a software package called QUALIKIN on a 386 micro-computer. The application of the statistical quality control methods and testing of the software was performed on two GPS data sets collected in land semi-kinematic mode over a well-controlled traverse. Analysis of the results indicates that, with a data rate of one second or higher, the testing procedure developed herein can correctly detect, identify and estimate carrier phase cycle slips between consecutive epochs occurring at the one cycle level on multiple satellites under low and medium vehicle dynamics. The detection and adaptation of phase rate and pseudorange outliers is also possible. The magnitude of the detectable outliers is dependent on the corresponding measurement accuracy, satellite geometry and the number of the outliers present. Further studies

of quality control methods are recommended. Among them are the extension of the testing procedure to incorporate the system bias detection and adaptation for high dynamic surveying and navigation systems, application of the theory to integrated systems such as GPS/INS, and investigation of the carrier phase ambiguity initialization methods in the kinematic mode.

## **ACKNOWLEDGMENTS**

I would like to express my deep gratitude to my supervisor, Professor Gerard Lachapelle, for his continuous support and encouragement throughout the course of my graduate studies. His advice and guidance were essential for the completion of this thesis.

Special thanks go to Dr. M.E. Cannon and Dr. Ming Wei, for their willingness to discuss GPS data processing techniques and problems related to my research. Mr. Bryan Townsend is sincerely thanked for sharing his knowledge in GPS and computer systems. He and Binbin She are also thanked for helping me in the field tests. Ms Caroline Erickson is gratefully acknowledged for carefully proofreading the manuscript. Finally, I wish to extend my appreciation to the Faculty, staff and fellow graduate students of the Department of Surveying Engineering for making my studies productive and enjoyable.

Financial support for this research came from The University of Calgary in the form of Graduate Teaching and Research Assistantships and the Helmut Moritz scholarship fund. Their contribution is gratefully acknowledged.

## TABLE OF CONTENTS

	<b>Page</b>
ABSTRACT .....	iii
ACKNOWLEDGEMENTS .....	v
TABLE OF CONTENTS .....	vi
LIST OF TABLES .....	ix
LIST OF FIGURES .....	x
NOTATION .....	xii
CHAPTER	
1 INTRODUCTION .....	1
1.1 Background .....	1
1.2 Outline of Thesis .....	3
2 THEORY OF QUALITY CONTROL IN KALMAN FILTERING .....	4
2.1 General Description .....	5
2.2 Two-stage Kalman Filter .....	7
2.2.1 Bias-free Kalman Filtering .....	8
2.2.2 Two Step Estimation of State Vector and Bias Vector .....	10
2.3 Testing Procedures and Reliability Measures in Kalman Filtering .....	15
2.3.1 Testing Statistics for Biases .....	15
2.3.2 Reliability Measures in Kalman Filtering .....	19
2.3.3 Testing Procedures .....	21
3 KINEMATIC DIFFERENTIAL GPS POSITION AND VELOCITY ESTIMATION MODEL .....	25
3.1 System Models .....	26

3.1.1	Constant Velocity Model .....	26
3.1.2	Constant Acceleration Model .....	28
3.2	Observation Model .....	30
4	RELIABILITY ANALYSIS IN KINEMATIC DIFFERENTIAL GPS SURVEYS .....	34
4.1	Bias Influences on Position and Velocity Estimation in Kinematic Differential GPS Surveys .....	34
4.2	MDB in Kinematic Differential GPS Surveying Model .....	45
5	CARRIER PHASE AMBIGUITY INITIALIZATION FOR DIFFERENTIAL KINEMATIC GPS SURVEYING .....	51
5.1	Phase Ambiguity Initialization in State Mode .....	52
5.2	Phase Ambiguity Initialization in Kinematic Mode .....	54
5.2.1	Ambiguity Function .....	55
5.2.2	Results of Phase Initialization by Ambiguity Function .....	58
6	TESTING AND RESULTS .....	64
6.1	Description of the Program QUALIKIN .....	64
6.2	Description of the Field Tests .....	68
6.3	Positioning Results .....	70
6.3.1	Day 222 Results .....	70
6.3.2	Day 121 Results .....	74
6.4	Detection and Adaptation for Simulated Biases .....	75
6.4.1	Detection and Adaptation for Simulated Cycle Slips .....	76
6.4.2	Detection and Adaptation for Simulated Outliers in Phase Rate Observations .....	82
6.4.3	Detection and Adaptation for Simulated Outliers in Pseudoranges Observation.....	84
7	CONCLUSIONS AND RECOMMENDATIONS .....	86
	REFERENCES .....	90

## LIST OF TABLES

<b>Table</b>	<b>Page</b>
5.1 Resolved Initial Phase Ambiguities by the AFM Using 5 Epochs of Observations from the Data Set of Day 121, 1991 .....	59
5.2 Resolved Phase Ambiguities by the AFM in Kinematic Mode Using One Epoch of Observations on Day 222, 1990 .....	60
5.3 Resolved Phase Ambiguities by the AFM in Kinematic Mode Using Two Epochs of Observations on Day 121, 1991 .....	62
6.1 Observation Information for the Semi-Kinematic Tests .....	69
6.2 Results of Cycle Slip Detection and Estimation for Simulated Cycle Slips in the Data Set of Day 121, 1991 (1 Second Data Rate) .....	77
6.3 Results of Cycle Slip Detection and Estimation for Simulated Cycle Slips in the Data Set of Day 222, 1990 (4 Seconds Data Rate) .....	79
6.4 Results of Bias Detection and Estimation for Simulated Phase Rate Outliers in the Data Set of Day 121, 1991 (1 Seconds Data Rate) .....	83
6.5 Results of Bias Detection and Estimation for Simulated Pseudorange Outliers in the Data Set of Day 121, 1991 (1 Seconds Data Rate) .....	85

## LIST OF FIGURES

<b>Figure</b>	<b>Page</b>
2.1 Process of Quality Control in Dynamic Systems .....	5
2.2 Flowchart of the Testing Procedure for Use in Kalman Filters .....	24
4.1 Dilution of Precision for Part of the Trajectory of Day 222, 1990 .....	36
4.2 Cycle Slip Influences on Positions and Velocities. Six Satellites (SVs 2, 6, 9, 11, 13, 18) are available simultaneously. SV 11 is assumed to have one cycle slip (19.02) starting from 494132 seconds. The data interval is 4 seconds .....	37
4.3 Cycle Slip Influences on Positions and Velocities. Six Satellites (SVs 2, 6, 9, 11, 13, 18) are available simultaneously. Two satellites (SVs 11, 18) are assumed to have two cycles slip starting from 494132 seconds. The data interval is 4 seconds .....	38
4.4 Pseudorange Outlier Influences on Positions and Velocities. Six Satellites (SVs 2, 6, 9, 11, 13, 18) are in view simultaneously. A single outlier of 20 m is assumed in the pseudorange of SV 11 at 494132 seconds. The data interval is 4 seconds .....	40
4.5 Phase Rate Outlier Influences on Positions and Velocities. Six Satellites (SVs 2, 6, 9, 11, 13, 18) are available simultaneously. A single outlier of $0.5 \text{ m s}^{-1}$ in the phase rate occurs on SV 11 at 494132 seconds. The data interval is 4 seconds .....	42
4.6 System Bias Influences on Predicted Positions and Velocities. An acceleration bias of $2 \text{ m s}^{-1}$ occurs on the system state $V_n$ at 6 consecutive epochs from time 494132 to 494152. The data interval is 4 seconds .....	44
4.7 Local MDB Improvement in Double Difference on Carrier Phase Observations on SV 02 with the Different Satellite Coverages .....	47
4.8 GDOP Improvement with the Different Satellite Coverages .....	47
4.9 Local MDB Improvements in Double Difference on Phase Rate Observations on SV 02 with the Different Satellite Coverages .....	48
4.10 Local MDB Improvements in Double Difference Pseudorange Observations on SV 02 with the Different Satellite Coverages .....	49
6.1 Flowchart of the Main Processor of the Program QUALIKIN .....	66

6.2	Sketch of the Test Traverse Control Points .....	68
6.3	Position Differences with the Control Points for Day 222, 1990 .....	71
6.4	Differences Between QUALIKIN and Ashtech KINSRVY for Kinematic Results of Day 222, 1990 .....	73
6.5	Position Differences with the Control Points for Day 121, 1991 .....	74
6.6	Comparison of the Results with and without Cycle Slip Adaptation for the Single Cycle Slip Case .....	81

## NOTATION

### i) Symbols

$a_n$	north acceleration
$a_e$	east acceleration
$a_h$	up acceleration
$\mathbf{b}$	bias vector
$\mathbf{b}_0$	minimum detectable bias vector with power $1-\beta_0$
$B, C$	influence matrices that determine how the bias vector $\mathbf{b}$ enters into the Kalman system and observation equations, respectively
$c$	speed of light
$d$	degree of freedom in chi-square distribution, number of biases
$e$	observation noise
$e^{i\theta}$	phasor or complex vector $e^{i\theta} = \cos\theta + i \sin\theta$
$H$	design matrix
$H_0$	null hypothesis
$H_a$	alternative hypothesis
$H_k$	Kalman gain matrix
$m$	Dimension of the innovation vector at each epoch, or number of update observations at each epoch
$N$	carrier phase ambiguity
$N(0, Q)$	normal probability distribution with expectation 0 and covariance matrix $Q$
$p$	pseudorange observation (m)
$P$	Kalman state vector covariance matrix

$Q$	Kalman filter process noise covariance matrix
$Q_v$	covariance matrix of innovation vector
$R$	Kalman filter observation noise covariance matrix
$R$	earth radius
$S$	sensitivity matrix related to the innovation vector
$T_G$	global model test statistic
$T_G^f$	global failure test statistic
$T_G^L - f$	local failure test statistic
$t_g^L$	local identification test statistic
$U$	sensitivity matrix related to the predicted Kalman state vector
$V$	sensitivity matrix related to the updated Kalman state vector
$v$	innovation vector, or predicted residual vector
$V_n$	north velocity
$V_e$	east velocity
$V_h$	up velocity
$w$	process noise
$x$	state vector
$z$	observation vector
$\alpha$	significance level or Type I error
$\alpha$	inverse of correlation time of the stochastic Markov process
$\beta$	Type II error
$1-\beta$	power of test
$\lambda$	non-centrality parameter in chi-square distribution
$\lambda$	L1 GPS carrier wavelength
$\lambda_0$	critical value of $\lambda$ which satisfies the given power $1-\beta_0$ and significance level $\alpha_0$

$\Phi$	Kalman filter transition matrix
$\Phi$	carrier phase observations (m)
$\chi^2(d,\lambda)$	chi-square probability distribution
$\phi$	geodetic latitude
$\lambda$	geodetic longitude
$h$	geodetic height
$\rho$	range from receiver to satellite
$\nabla\Delta N$	double difference carrier phase ambiguity

## ii) Defined Operators

(+)	Kalman update
(-)	Kalman prediction
$\Phi$	derivative with respect to time
$H^T$	matrix transpose
$Q^{-1}$	matrix inverse
$\Delta$	single difference between receivers
$\nabla$	single difference between satellites
$\nabla$	deviation in
$\delta$	correction to
$\hat{x}$	bias-free or bias-ignored Kalman filter estimated value
$\tilde{x}$	bias-corrected Kalman filter estimated value
$ \cdot $	norm operator
$\sim$	distributed as

### iii) Acronyms

AFM	Ambiguity Function Method
AVL	Automatic Vehicle Location
C/A code	Clear / Acquisition code
DD	Double Difference
DGPS	Differential GPS
GDOP	Geometry Dilution of Precision
GPS	Global Positioning System
GMT	Global Model Test
HDOP	Horizontal Dilution of Precision
INS	Inertial Navigation System
LBNR	Local Bias-to-Noise Ratio
LMT	Local Model Test
MDB	Minimum Detectable Bias
P code	Precise code
RMS	Root Mean Square
SD	Single Difference
SV	Space Vehicle
TD	Triple Difference
VDOP	Vertical Dilution of Precision

## CHAPTER 1

### INTRODUCTION

#### 1.1 BACKGROUND

Kinematic surveying with the Global Positioning System (GPS) plays a key role in a number of positioning activities, such as precise navigation, airborne gravimetry and gradiometry, airborne photogrammetry and Automatic Vehicle Location (AVL). With the full deployment of 24 GPS satellites in the near future and the improved receiver technologies (e.g., all-in-view satellite receivers), kinematic GPS surveys, which include the determination of position, velocity or even acceleration of a moving platform, may become a routine job for geodesists and surveyors. As we know from conventional geodetic surveys, the quality assessment of surveying results generally involves accuracy analysis, reliability analysis and statistical testing of the estimated quantities and adequacy of the adjustment model. Accuracy analysis deals with the propagation of random errors through the geometric strength of the network or the adjustment model, while reliability analysis and statistical testing, which are the primary elements of quality control, deal with the self-check ability of the model or system to blunders or biases that occur in observations or in the systems. Up to now, extensive investigations and tests have been done in the accuracy analysis of kinematic differential GPS surveys. The results of 0.2m (standard deviation) in kinematic positioning and 0.05m/s

(standard deviation) in velocity estimation have been made by using both pseudorange and carrier phase observations (Lachapelle et al, 1989; Schwarz et al, 1989; Cannon, 1987). The reliability analysis and statistical testing in kinematic GPS surveys, however, is just at its initial stage. Teunissen and Salzmänn (Teunissen, 1990; Salzmänn and Teunissen, 1989) introduced the quality control concept of conventional geodetic surveys into kinematic surveying systems and developed the general quality control theory based on the standard state space Kalman filtering model and the statistical hypothesis testing. The first application and adaptation of this theory to kinematic GPS positioning was given by Wei et al (Wei et al,1990) and Lu and Lachapelle (Lu and Lachapelle,1990).

It is known that by using GPS pseudorange, carrier phase and phase rate (Doppler) observations in a Kalman filter, the instantaneous position, velocity and even acceleration of a moving platform can be determined (Schwarz et al,1989; Cannon,1990; Hwang and Brown, 1990). If the assumed dynamic and observation models are correct, the Kalman filter provides the optimal position and velocity estimates in a statistical sense. In a dynamic environment, however, the deviations or biases from the assumed models are often significant. For instance, the loss/re-lock of a carrier phase signal on a satellite will cause the corresponding integrated carrier phase observations to jump abruptly, which falsifies the measurement update model. Likewise, a pre-determined constant velocity model for vehicle motion may be invalidated due to high vehicle accelerations in some parts of the trajectory. Such deviations or biases will certainly lead to some errors in the filtering results. Therefore, reliability analysis and real-time testing and adaptation for possible biases is of great importance in kinematic GPS surveys in order to prevent the degradation of position and velocity estimates.

## 1.2 OUTLINE OF THESIS

The primary objective of this thesis is to apply the quality control methods to kinematic GPS surveys. The general formulas and procedures for reliability analysis and bias detection and adaptation in Kalman filtering are derived. A software package, QUALIKIN, that performs reliability analysis, real-time statistical testing and adaptation for possible biases in pseudo-range, carrier phase and phase rate observations along with kinematic differential GPS positioning and/or semi-kinematic positioning, is developed.

Chapter 2 describes the quality control theory of the state space Kalman filtering. Firstly, a more general recursive bias influence formulation on filtered quantities is introduced by using a two-stage Kalman filter method. Then, a real-time statistical testing procedure for use in the Kalman filter is given based on the hypothesis testing theory and the Minimum Detectable Bias (MDB) concept. The system model and the observation model for kinematic positioning used in this research are outlined in Chapter 3. Chapter 4 investigates the influence characteristics of different biases (e. g., cycle slips) on kinematic positioning results and the corresponding minimum detectable biases. In Chapter 5, methods for carrier phase ambiguity initialization are reviewed. In particular, the ambiguity function method (Mader, 1990) is discussed and tested for phase ambiguity resolution in kinematic mode. The processing results of real data sets and the applicability of statistical methods for detecting and correcting biases in observations are listed in Chapter 6. Some conclusions and recommendations are given in Chapter 7.

## CHAPTER 2

### **THEORY OF QUALITY CONTROL IN KALMAN FILTERING**

The quality control method, i.e. reliability analysis and statistical testing of the adequacy of adjustment models, has been widely used for network design and data processing in conventional geodesy, photogrammetry and surveying (Baarda, 1968; Li, 1986; Pelzer, 1986). In systems engineering, it is often called fault detection, diagnosis and adaptation (Basseville,1988; Frank,1990). With the advent of the global positioning system (GPS), kinematic surveying is now becoming a recognized surveying method on land, in the air and on the sea. Therefore, it is natural and important to introduce and apply the quality control method to this new kinematic surveying method to insure the correctness of the results obtained.

In this chapter, the general concept of quality control in dynamic systems engineering is reviewed first. Then, two-stage Kalman filter formulas are derived, which are useful for analyzing the bias influence on Kalman filter output quantities. And finally, the formulation of testing procedures and reliability analysis is presented.

## 2.1 GENERAL DESCRIPTION

The process of quality control or fault detection, diagnosis and adaptation in dynamic systems essentially consists of three stages (Basseville,1988; Teunissen,1990): residual generation, decision making and adaptation or estimation, as shown in Fig. 2.1.

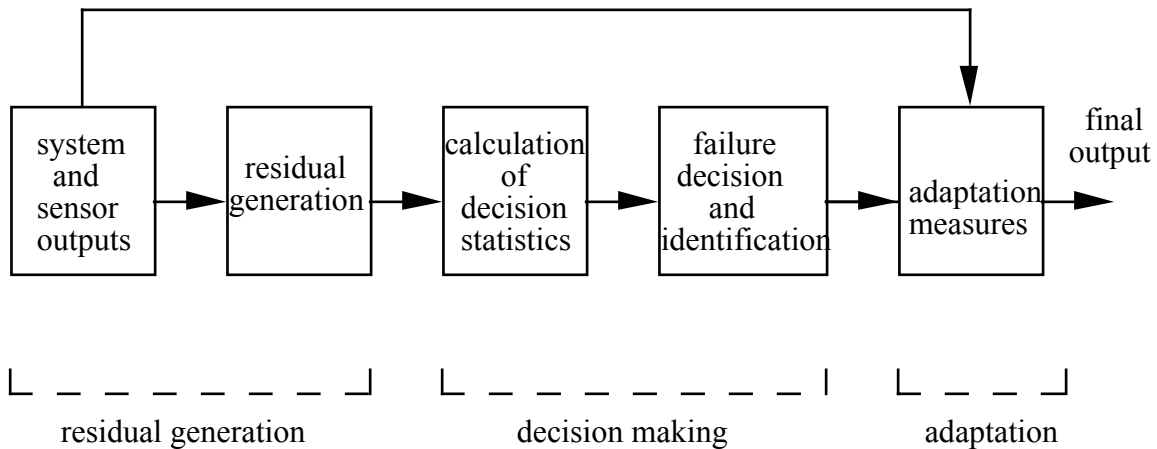


Fig. 2.1 Process of Quality Control in Dynamic Systems

The residual generation is based on the knowledge of the normal behaviour of the system and the characteristics of the failures. For detection purposes, constructed residuals should significantly and quickly reflect the influences of possible failures or biases which occurred in the analyzed system, and remain unbiased, normally close to zero, in the absence of failures or biases. In kinematic surveying systems like GPS and Inertial Navigation Systems (INS), Kalman filtering is widely used for data processing. In this case, one suitable choice of residual generation is the filter output of innovation sequence, i.e. predicted residuals (Willsky, 1976; Teunissen, 1990). The generation of innovation sequence and its properties are given in Section 2.2.

Decision making is the construction of decision functions or test statistics based on the generated residuals. Decision functions or statistics are then calculated using the residuals to determine if any failure has occurred in the system. In some cases, failure identification or isolation should also be carried out. For innovation-based detection systems like Kalman filters, a number of statistical tests to be performed on the innovations have been suggested. Among them are the Chi-square statistic and the Generalized Likelihood Ratio (GLR) test (Teunissen, 1990; Willsky, 1976; Mehra and Peschon, 1971). Due to its simplicity and easy implementation, the real-time Chi-square test is used in this research for detecting and isolating the possible biases (e.g., cycle slips on some satellites) in the kinematic GPS surveying model.

Adaptation is system reconfiguration to accommodate the failure, or to estimate the failure or bias and then correct its influences on system outputs. Reconfiguration measures are often used in a system with a high degree of parallel hardware redundancy (e.g., voting system), while analytical correction methods are usually adopted in a single feedback system. For kinematic surveying with a single GPS system, only real-time analytical correction methods are possible. For this purpose, two-stage Kalman filter techniques are derived for real-time bias estimation and correction.

Another important aspect of quality control is the *reliability analysis* of the systems. This concept was mainly developed by geodetic scientists (Baarda, 1968; Teunissen, 1990) and has not yet been discussed in system engineering literature. Generally speaking, reliability is concerned with the self-checking ability of the system model for possible biases and the effects of undetectable biases on the estimated results. One of the numerical measures for reliability in dynamic systems is the *minimum detectable bias* (MDB) (Teunissen, 1990), which is the minimum bias value that can be detected with a certain probability by a specified bias testing statistic in an  $\alpha$  level test. The importance of reliability analysis lies in the design stage of a dynamic system. By examining the reliabilities of different design schemes, an efficient

system with sufficient control on the presence of certain biases can be obtained. In kinematic GPS surveys, for instance, the reliability analysis can be conveniently used for investigating the minimal detectable cycle slips occurring on a certain satellite and the cycle slips effect on position and velocity determination. This problem and the application of reliability analysis in kinematic differential GPS surveys will be discussed in Chapter 4.

## **2.2 TWO-STAGE KALMAN FILTER**

Under the nominal conditions that the system and observation model and the statistical model are correct, the Kalman filter provides estimates of the state vector which are unbiased and of minimum variance. Due to the dynamic environment and possible failures of some system components, deviations or biases from the predetermined filter model are often encountered in practice. An important class of biases, which is suitable to represent cycle slips in carrier phase measurements and outliers in pseudorange and phase rate observations, are the *constant biases* with unknown magnitudes. Usually, there are two ways to treat these kinds of biases when they are detected in the system dynamic model or the observation model. Firstly, one can augment the state vector of the original model by adding components to represent the bias terms. The filter then estimates these terms as well as the original states. This mechanism, for example, is implemented in the well-known program SEMIKIN for estimating the cycle slips in carrier phase measurements (Cannon, 1990). Secondly, the bias terms can be estimated separately from the original filter states by using the bias-free, i.e. the nominal Kalman filtering results. This is the so-called two-stage Kalman filter (Friedland, 1969; Ignagni, 1981). Mathematically, these two methods are equivalent. However, the second method has the advantages of being computationally efficient and convenient for both bias influence analysis and reliability analysis of filtering results. Therefore, it is used in this research for reliability analysis and processing software development.

## 2.2.1 Bias-free Kalman Filtering

The general Kalman filter equations are well documented in Gelb (1974). For a system described by the following equations

$$x_k = \Phi_k x_{k-1} + w_k, \quad w_k \sim N(0, Q_k) \quad (2.1)$$

$$z_k = H_k x_k + e_k, \quad e_k \sim N(0, R_k), \quad (2.2)$$

the optimal estimate of the state vector  $x_k$  and its covariance matrix are given by

$$\text{Prediction:} \quad \hat{x}_k(-) = \Phi_k \hat{x}_{k-1}(+) \quad (2.3)$$

$$P_k(-) = \Phi_k P_{k-1}(+) \Phi_k^T + Q_k \quad (2.4)$$

$$\text{Update:} \quad \hat{x}_k(+) = \hat{x}_k(-) + K_k [z_k - H_k \hat{x}_k(-)] \quad (2.5)$$

$$P_k(+) = [I - K_k H_k] P_k(-) \quad (2.6)$$

$$K_k = P_k(-) H_k^T [H_k P_k(-) H_k^T + R_k]^{-1} \quad (2.7)$$

where (-) denotes the predicted quantities, i.e., before update,

(+) denotes the updated quantities,

$x_k$  is the state vector,

$\Phi_k$  is the transition matrix,

$P_k$  is the state covariance matrix,

$K_k$  is the Kalman gain matrix,

$Q_k$  is the covariance matrix of the system process noise  $w_k$ ,

$R_k$  is the covariance matrix of the observation noise  $e_k$ ,

$H_k$  is the design matrix,

and  $z_k$  is the observation vector for updating.

If the equations (2.1) and (2.2) correctly specify the underlying system model and observation model, the Kalman algorithm from equations (2.3) to (2.7) gives the minimum variance, unbiased estimate of the state vector  $x$  at each epoch  $k$ . In this case, the *innovations*, i.e. the predicted residuals  $v_k$  described as

$$v_k = z_k - H_k \hat{x}_k(-) \quad (2.8)$$

have a zero mean, Gaussian white noise sequence with covariance matrix

$$Q_{v_k} = R_k + H_k P_k(-) H_k^T \quad (2.9)$$

(Mehra and Peschon, 1971; Willsky, 1976; Teunissen, 1989). Any deviation or bias arising from the system model (2.1) or from the observation model (2.2) may cause the innovation sequence (2.8) to depart from its zero mean and whiteness properties. This makes the innovation sequence an ideal *generated residual* sequence in Kalman filtering for detecting the abnormal behaviours of the system.

### 2.2.2 Two Step Estimation of State Vector and Bias Vector

In the presence of constant biases with unknown magnitudes in the functional model of Kalman filtering, equations (2.1) and (2.2) can be reformulated as:

$$x_k = \Phi_k x_{k-1} + B_k \mathbf{b} + w_k, \quad w_k \sim N(0, Q_k) \quad (2.10)$$

$$z_k = H_k x_k + C_k \mathbf{b} + e_k, \quad e_k \sim N(0, R_k), \quad (2.11)$$

where  $\mathbf{b}$  is the constant bias vector. The matrices  $B_k$  and  $C_k$  determine how the components of the bias vector  $\mathbf{b}$  enter into the dynamics and observations respectively. In the case when

only observations have biases,  $B_k = 0$ . Similarly, if only the dynamics have biases,  $C_k = 0$ . If no biases present in the model,  $B_k = C_k = 0$ .

In *one step* (simultaneous) estimation, the bias vector  $\mathbf{b}$  in (2.10) and (2.11) is appended to the original state vector  $\mathbf{x}$  with the dynamics  $\mathbf{b}_k = \mathbf{b}_{k-1}$  to form a new state vector  $\mathbf{y} = (\mathbf{x}, \mathbf{b})$ . Then, the new state vector  $\mathbf{y}$  is estimated by the conventional Kalman algorithm (2.3) to (2.7) based on the augmented model

$$\mathbf{y}_k = F_k \mathbf{y}_{k-1} + G \mathbf{w}_k, \quad \mathbf{w}_k \sim N(0, Q_k) \quad (2.12)$$

$$\mathbf{z}_k = L_k \mathbf{y}_k + \mathbf{e}_k, \quad \mathbf{e}_k \sim N(0, R_k) \quad (2.13)$$

with the partitioned matrices

$$F_k = \begin{pmatrix} \Phi_k & B_k \\ 0 & I \end{pmatrix}, \quad G = \begin{pmatrix} I \\ 0 \end{pmatrix}, \quad L_k = (H_k, C_k). \quad (2.14)$$

This method preserves the mathematical simplicity, but has the disadvantages that it increases the dimension of the state vector and is not suitable for reliability analysis and bias influence analysis in Kalman filtering.

The two step estimation of states and biases overcomes the disadvantages in the above one step estimation procedure. The basic idea for two step estimation of states  $\mathbf{x}$  and biases  $\mathbf{b}$  is as follows. In the first step, we ignore the bias terms in (2.10) and (2.11), and perform the conventional bias-free Kalman filtering procedure. Due to the omission of bias terms, we then obtain the biased state estimates,  $\hat{\mathbf{x}}_k(+)$  and  $\hat{\mathbf{x}}_k(-)$ , and the biased innovations  $\mathbf{v}_k$  that contain the information on the biases. In the second step, the bias vector  $\mathbf{b}$  is estimated by using the innovations obtained in the first step, and the biased state estimates,  $\hat{\mathbf{x}}_k(+)$  and  $\hat{\mathbf{x}}_k(-)$ , are corrected for the bias influences. Mathematically, two step estimation of states and biases is equivalent to one step estimation. The proof is given by Friedland (1969) and Ignagni (1981).

Here, only an intuitive derivation is given and the emphasis is placed on the computational aspects.

**a. Bias influences on bias-free state estimates**

If the bias vector were perfectly known, as is the case when we analyse the influence of a specified bias vector on the Kalman filtering results, the optimal estimates of the state vector  $x$  in equations (2.10) and (2.11) would be

$$\tilde{x}_k(-) = \Phi_k \tilde{x}_{k-1}(+) + B_k \mathbf{b} \quad (2.15)$$

$$\tilde{x}_k(+) = \tilde{x}_k(-) + K_k (z_k - H_k \tilde{x}_k(-) - C_k \mathbf{b}) , \quad (2.16)$$

while the innovations with known biases would be

$$\tilde{v}_k = z_k - H_k \tilde{x}_k(-) - C_k \mathbf{b} , \quad (2.17)$$

where  $\mathbf{b}$  is the true value of the constant bias vector,  $K_k$  is the Kalman gain matrix defined by (2.7) of the bias-free model, and  $\tilde{x}_k(-)$  and  $\tilde{x}_k(+)$  are the *bias-corrected* Kalman state estimates before and after update, respectively.

Since the Kalman filter estimator is a linear estimator and the bias influence on the filter estimates, as reflected in (2.16) and (2.17), is also linear in nature, we can formally write the relationships between the bias-ignored estimates  $\hat{x}_k(-)$  and  $\hat{x}_k(+)$  and bias-corrected estimates  $\tilde{x}_k(-)$  and  $\tilde{x}_k(+)$  as (Friedland, 1969):

$$\tilde{x}_k(-) = \hat{x}_k(-) + U_k \mathbf{b} \quad (2.18)$$

$$\tilde{x}_k(+) = \hat{x}_k(+) + V_k \mathbf{b} . \quad (2.19)$$

For the same reason, the relationship between the corresponding bias-ignored innovations  $v_k$  and the bias-corrected innovations  $\tilde{v}_k$  can be written as

$$v_k = \tilde{v}_k + S_k \mathbf{b} , \quad (2.20)$$

where  $U_k$ ,  $V_k$  and  $S_k$  are called *sensitivity matrices*. Equations (2.18), (2.19) and (2.20) indicate that in the presence of biases, the optimal Kalman filter state (bias-corrected) estimates can be obtained by adding corrections to the bias-free or bias-ignored Kalman filter estimates.

Substituting equations (2.15), (2.3) and (2.19) into (2.18), we obtain the recursive form for computing  $U_k$  :

$$U_k = \Phi_k V_{k-1} + B_k \quad (2.21)$$

Similarly, the recursive forms for  $V_k$  and  $S_k$  can be derived as:

$$V_k = U_k - K_k S_k \quad (2.22)$$

$$S_k = H_k U_k + C_k . \quad (2.23)$$

The initial value for the recursive computations of  $U_k$ ,  $V_k$  and  $S_k$  starting at epoch  $k$  is  $V_{k-1} = 0$  in equation (2.21). It is noted that the computations of  $U_k$ ,  $V_k$  and  $S_k$  are independent of the measurements. They can be computed beforehand using the specified dynamics model, observation model and bias type. Equations (2.21), (2.22) and (2.23) are of great importance in bias influence analysis. If a bias occurs in the system, its influence on the bias-free Kalman filtering estimates  $\hat{x}_k(-)$ ,  $\hat{x}_k(+)$  and  $v_k$ , as shown in (2.21), (2.22) and (2.23), are  $-U_k \mathbf{b}$ ,  $-V_k \mathbf{b}$  and  $S_k \mathbf{b}$  respectively. In kinematic GPS surveys, the most likely biases are carrier phase cycle slips, outliers in pseudorange and phase rate observations, and the deviations of the vehicle motion from the assumed dynamics. Their influence on kinematic GPS position and velocity determination is to be investigated in Chapter 4.

## **b. Bias estimation**

In real data processing, the true value of the bias vector  $\mathbf{b}$  is usually unknown. It is required that the bias vector be estimated in real time in order to correct its influences on the filtering results. This can be achieved by utilizing the equation (2.20). Rewriting (2.20) in the form:

$$\mathbf{v}_k = \mathbf{S}_k \mathbf{b} + \tilde{\mathbf{v}}_k \quad , \quad (2.24)$$

the bias-free Kalman filter innovations  $\mathbf{v}_k$  can then be considered as a quasi-measurement vector,  $\mathbf{S}_k$  as a design matrix and  $\tilde{\mathbf{v}}_k$ , the bias-corrected innovations, as the quasi-measurement noise. Based on the properties of Kalman filtering and equation (2.17), the bias-corrected innovation sequence  $\tilde{\mathbf{v}}_k$  is a white noise sequence with the covariance matrix at each epoch:

$$\mathbf{Q}_{\tilde{\mathbf{v}}_k} = \mathbf{H}_k \mathbf{P}_k(-) \mathbf{H}_k^T + \mathbf{R}_k, \quad (2.25)$$

where  $\mathbf{P}_k(-)$  is given by equation (2.4).

From the above discussions, it is obvious that the bias vector  $\mathbf{b}$  can be recursively estimated with a Kalman filter algorithm or an equivalent sequential least squares method using the measurement equation defined by (2.24) with the measurement white noise covariance matrix (2.25). The Kalman filter algorithm for recursive estimation of the bias vector  $\mathbf{b}$  has the form

$$\hat{\mathbf{b}}^{(-)}(k) = \hat{\mathbf{b}}^{(+)}(k-1) \quad ( \hat{\mathbf{b}}_0 = \mathbf{0} ) \quad (2.26)$$

$$\mathbf{P}_b^{(-)}(k) = \mathbf{P}_b^{(+)}(k-1) \quad ( \mathbf{P}_b(0) \text{ given} ) \quad (2.27)$$

$$\hat{\mathbf{b}}^{(+)}(k) = \hat{\mathbf{b}}^{(-)}(k) + \mathbf{K}_b(k) [ \mathbf{v}_k - \mathbf{S}_k \hat{\mathbf{b}}^{(-)}(k) ] \quad (2.28)$$

$$\mathbf{P}_b^{(+)}(k) = [ \mathbf{I} - \mathbf{K}_b(k) \mathbf{S}_k ] \mathbf{P}_b^{(-)}(k) \quad (2.29)$$

$$\mathbf{K}_b(k) = \mathbf{P}_b^{(-)}(k) \mathbf{S}_k^T [ \mathbf{S}_k \mathbf{P}_b^{(-)}(k) \mathbf{S}_k^T + \mathbf{H}_k \mathbf{P}_k(-) \mathbf{H}_k^T + \mathbf{R}_k ]^{-1} \quad (2.30)$$

This constitutes the second stage of two-stage Kalman filtering, i.e. bias estimation. It is noted from equation (2.30) that we need to invert a matrix of dimension that is equal to the number of observations at each epoch. In the kinematic GPS positioning model, the number of biases is usually smaller than the number of observations at each epoch. Therefore, the equivalent Bayes form or phase expressions (Krakiwsky, 1990) are more favourable than the Kalman algorithm given by (2.26) through (2.30), since the Bayes form inverts a matrix of dimension that is equal to the number of biases.

### c. Bias influence correction and adaptation

According to equations (2.18) and (2.19), once the bias estimates are obtained, the bias-ignored Kalman filter estimates,  $\hat{\mathbf{x}}_k^{(-)}$  and  $\hat{\mathbf{x}}_k^{(+)}$ , and their covariance matrices can be recursively corrected for the bias influences by:

$$\tilde{\mathbf{x}}_k^c(-) = \hat{\mathbf{x}}_k(-) + \mathbf{U}_k \hat{\mathbf{b}}^{(-)}(k) \quad (2.31)$$

$$\tilde{\mathbf{x}}_k^c(+) = \hat{\mathbf{x}}_k(+) + \mathbf{V}_k \hat{\mathbf{b}}^{(+)}(k) \quad (2.32)$$

$$\tilde{\mathbf{P}}_k^c(-) = \mathbf{P}_k(-) + \mathbf{U}_k \mathbf{P}_b^{(-)}(k) \mathbf{U}_k^T \quad (2.33)$$

$$\tilde{\mathbf{P}}_k^c(+) = \mathbf{P}_k(+) + \mathbf{V}_k \mathbf{P}_b^{(+)}(k) \mathbf{V}_k^T \quad (2.34)$$

$$\tilde{\mathbf{P}}_{xb}^{(-)}(k) = \mathbf{U}_k \mathbf{P}_b^{(-)}(k) \quad (2.35)$$

$$\tilde{\mathbf{P}}_{xb}^{(+)}(k) = \mathbf{V}_k \mathbf{P}_b^{(+)}(k) \quad (2.36)$$

where  $\tilde{\mathbf{x}}_k^c(-)$ ,  $\tilde{\mathbf{x}}_k^c(+)$ ,  $\tilde{\mathbf{P}}_k^c(-)$ ,  $\tilde{\mathbf{P}}_k^c(+)$  are the optimal unbiased state estimates and their corresponding covariance matrices, which have taken into account the influence of the biases in the models. In the derivation of (2.33) to (2.36), the fact that the state vector  $\mathbf{x}$  initially and at all subsequent epochs is uncorrelated with the biases  $\mathbf{b}$  has been used.

## **2.3 TESTING PROCEDURES AND RELIABILITY MEASURES IN KALMAN FILTERING**

### **2.3.1 Testing statistics for biases**

Failure detection and identification are the most important and yet the most difficult aspects in the quality control of Kalman filtering. Generally speaking, failures or malfunctioning of a Kalman filter may be caused by two error sources. One is the errors arising from the function models, such as the unmodelled biases in the measurements and system dynamics. The other source is the errors arising from the stochastic models defined mainly by the covariance matrices of the system process noise  $w_k$  and the measurement noise  $e_k$ .

In differential (double difference) kinematic GPS surveying, the functional model errors, such as the cycle slips in carrier phases and the outliers in pseudoranges and phase rates, are frequent and have severe influences on position and velocity determination. The stochastic model errors, relatively speaking, are much less significant than the functional model errors. The measurement noise in a surveying session is mainly specified by the instrumentation and environment and can be considered as a constant (Lachapelle, 1990). The system process noise, on the other hand, is determined by the vehicle motion. In a low or medium dynamic surveying system, the first-order Gaussian-Markov model of constant velocity or constant acceleration of the vehicle motion seems justified (Schwarz et al, 1989; Cannon, 1990). In practical computations, we usually use slightly larger values for measurement variance and process noise spectral density to cope with the unpredictable statistical behaviors of the system. Therefore, in the following the statistical models of the Kalman filter are considered correct and the focus is placed on the detection and isolation of biases in the function models.

In order to develop the statistics for bias detection, we first define a vector consisting of  $n+1$  epochs of innovations of equation (2.8)

$$\mathbf{v} = (v_1, v_{l+1}, v_{l+2}, \dots, v_{l+n})^T. \quad (2.37)$$

As we know from section 2.2, under normal conditions when the Kalman filter models are specified correctly and no biases are present, the innovation sequence is a zero mean, Gaussian white noise sequence. In this case, vector  $\mathbf{v}$  has a normal distribution

$$\mathbf{v} \sim N(0, Q_v), \quad (2.38)$$

where  $Q_v$  is a block-diagonal matrix since the innovations are uncorrelated from epoch to epoch (Teunissen and Salzmman, 1989). However, if a bias vector  $\mathbf{b}$  of dimension  $d$  is present in the functional models, the zero mean of the innovations at each epoch is no longer holds. Instead, the innovation sequence is biased, as known from (2.20), by a value  $S_k \mathbf{b}$ . This leads to

$$\mathbf{v} \sim N(\nabla \mathbf{v}, Q_v) \quad (2.39)$$

with  $\nabla \mathbf{v} = S_v \cdot \mathbf{b}, \quad (2.40)$

$$S_v = (S_l^T, S_{l+1}^T, \dots, S_{l+n}^T)^T, \quad (2.41)$$

where  $S_v$  is a  $(\sum_{i=1}^{l+n} m_i)$ -by- $d$  matrix and  $m_i$  is the dimension of  $v_i$ .

Thus, the problem of detection of the bias vector  $\mathbf{b}$  can be formulated as the testing of the null hypothesis  $H_0$  against the alternative hypothesis  $H_a$  :

$$H_0 : \mathbf{v} \sim N(0, Q_v) \quad \text{versus} \quad H_a : \mathbf{v} \sim N(\nabla \mathbf{v}, Q_v). \quad (2.42)$$

The testing statistic for the above problem (2.42) is well documented in a number of publications (Teunissen, 1986, 1990; Rao,1973 ) and is given by

$$T_G = \mathbf{v}^T \mathbf{Q}_v^{-1} \mathbf{S}_v (\mathbf{S}_v^T \mathbf{Q}_v^{-1} \mathbf{S}_v)^{-1} \mathbf{S}_v^T \mathbf{Q}_v^{-1} \mathbf{v} . \quad (2.43)$$

Since the matrix  $\mathbf{Q}_v$  is block diagonal, (2.43) can be further reduced to the summation form based on (2.37), (2.41):

$$T_G = \left( \sum_{i=1}^{1+n} \mathbf{S}_i^T \mathbf{Q}_{v_i}^{-1} \mathbf{v}_i \right)^T \left( \sum_{i=1}^{1+n} \mathbf{S}_i^T \mathbf{Q}_{v_i}^{-1} \mathbf{S}_i \right)^{-1} \left( \sum_{i=1}^{1+n} \mathbf{S}_i^T \mathbf{Q}_{v_i}^{-1} \mathbf{v}_i \right) . \quad (2.44)$$

Under the null hypothesis  $H_0$  ,  $T_G$  has a central  $\chi^2$  -distribution, i.e.

$$T_G \sim \chi^2(d, 0) \quad \text{under } H_0 , \quad (2.45)$$

while under the alternative hypothesis  $H_a$  ,  $T_G$  has a non-central  $\chi^2$  -distribution, i.e.

$$T_G \sim \chi^2(d, \lambda) \quad \text{under } H_a , \quad (2.46)$$

where  $d$  is the degrees of freedom which is equal to the number of biases and  $\lambda$  is the non-centrality parameter which is defined by

$$\lambda = \mathbf{b}^T \left( \sum_{i=1}^{1+n} \mathbf{S}_i^T \mathbf{Q}_{v_i}^{-1} \mathbf{S}_i \right) \mathbf{b} \quad (2.47)$$

The null hypothesis that there are no such biases  $\mathbf{b}$  present in the model is accepted if  $T_G$  is less than the upper  $\alpha$ -percentage point of the central  $\chi^2$  -square probability distribution  $\chi^2(d, 0)$  , i.e.

$$H_0 \text{ is accepted if } T_G \leq \chi_{\alpha}^2(d, 0) . \quad (2.48)$$

Otherwise,  $H_0$  is rejected in favour of  $H_a$  , meaning that the specified bias vector  $\mathbf{b}$  is statistically significant under the significance level or risk level  $\alpha$ .

The test statistic of (2.44) can be sub-divided into two cases. They are the so-called *local model test* (LMT) and *global model test* (GMT) (Teunissen and Salzmann, 1989). If only the current one epoch innovation is used to form the statistic (2.44), it is called a local test. This corresponds to  $n=0$  in (2.44). Otherwise, it is a global test which means that more than one epoch of innovations have been included in the computation of the statistic  $T_G$ . The main advantage of the global test is the better detection power for systematic model bias trend (Teunissen and Salzmann, 1989; Lu and Lachapelle, 1990). But we pay for it with increased computational complexity and time.

In real-time data processing, once a bias vector  $\mathbf{b}$  is detected and estimated, its effects on the bias-free Kalman filter results should be immediately corrected in order to prevent further deterioration in subsequent epochs. This can be done by the algorithms of the two-stage Kalman filter given in the previous subsection 2.2.2.

### 2.3.2 Reliability measures in Kalman filtering

When applying the statistical testing for certain postulated biases, we are likely to make two types of errors. A Type I error is the rejection of the null hypothesis  $H_0$  when it is true. The probability of making this type of error (false alarm) is the test significance level or risk level  $\alpha$ . A Type II error is the acceptance of  $H_0$  when the alternative hypothesis  $H_a$  is actually true. The probability of making type II errors is denoted by  $\beta$ , which is related to the non-centrality parameter  $\lambda$  of the alternative test distribution and the given significance level  $\alpha$ . Unfortunately, type I and type II errors can not be minimized at the same time. They are related through the non-centrality parameter of the alternative test distribution. By fixing any two of  $\alpha$ ,  $\beta$  and  $\lambda$ , the third one can be computed. Generally, the larger the non-centrality parameter of the alternative test distribution, the smaller the probability  $\beta$  of type II error or the

larger the *power*  $1-\beta$  of the statistical test. In this case, we may ask a question on how large the non-centrality parameter  $\lambda$  should be in order to satisfy a pre-determined power  $1-\beta_0$  of the statistical test associated with a significance level  $\alpha_0$ . This readily brings us to the important concept of reliability in geodetic science (Baarda, 1968; Pelzer, 1988, Teunissen, 1990).

Reliability is mainly concerned with the effects of possible biases in the model on the estimated results and the ability of the redundant information in the model to check against the model biases or misspecifications. In Kalman filtering, the influences of fixed biases on the filtering results can be easily investigated by using two-stage Kalman filter equations (2.18), (2.19) and (2.20), while the ability to detect the individual bias in the system, which is usually termed *internal reliability* in surveying, is measured with the quantity of minimum detectable bias (MDB).

Suppose  $\lambda_0$  is the minimum value of the non-centrality parameter which satisfies the given test power  $1-\beta_0$  and significance level  $\alpha_0$ . From (2.47), we immediately obtain the minimum detectable bias (MDB) vector  $\mathbf{b}_0$  as:

$$\lambda_0 = \mathbf{b}_0^T \left( \sum_{i=1}^{1+n} \mathbf{S}_i^T \mathbf{Q}_{v_i}^{-1} \mathbf{S}_i \right) \mathbf{b}_0 \quad . \quad (2.49)$$

For a single bias,  $\mathbf{b}_0$  is reduced to a scale and (2.49) can be written as

$$\mathbf{b}_0 = \sqrt{\frac{\lambda_0}{\sum_{i=1}^{1+n} \mathbf{S}_i^T \mathbf{Q}_{v_i}^{-1} \mathbf{S}_i}} \quad . \quad (2.50)$$

Equation (2.50) shows that the magnitude of a single bias should at least reach  $\mathbf{b}_0$  in order to be detected with the power  $1-\beta_0$  in an  $\alpha_0$  significance level test. This property is utilized in the testing procedures to be described in the next subsection.

The minimum detectable bias vectors corresponding to the Local Model Test and the Global Model Test are referred to as Local MDB and Global MDB vectors respectively. For multiple biases, the quadratic form (2.49) describes a hyper-ellipsoid if  $\lambda_o$  is held to a constant value. The axes of this hyper-ellipsoid are the inverses of the square roots of the eigenvalues of the matrix  $\sum_{i=1}^{l+n} (S_i^T Q_{v_i}^{-1} S_i)$  which has a dimension equal to the number of biases .

A number of tables have been provided for calculation of the non-centrality parameter  $\lambda_o$  (Caspar,1987; Baarda,1968) . For example, in a one-dimensional alternative hypothesis test (2.46) with the degrees of freedom equal to one,  $\lambda_o$  is equal to  $(4.13)^2$  when we set  $\beta_o = 20\%$  and  $\alpha_o = 0.1\%$  . The computation of  $S_i$  and  $Q_{v_i}^1$  , as known from the two-stage Kalman filter algorithm, is independent of the actual measurements. Hence, the MDB of a specified bias can be computed before the filter is actually implemented. This makes the MDB a useful tool in Kalman filter design. An efficient filter design with required reliability control on the postulated biases can be achieved by examining the different filter operation schemes.

### 2.3.3 Testing procedures

The test statistic (2.43) or (2.44) is aimed at detecting a specified bias vector  $\mathbf{b}$  of dimension  $d$  through the sensitivity matrix  $S_i$  . In a particular application, however, we are usually not sure beforehand when and what kind of biases will occur in the system. It is therefore necessary to establish testing statistics to detect first whether there is a failure or malfunctioning in the underlying filter operations or not. This can be realized by leaving the bias vector  $\mathbf{b}$  completely unspecified, that is, letting the dimension of the bias vector  $\mathbf{b}$  equal to the dimension of the innovations vector  $\mathbf{v}$  (Teunissen and Salzmann, 1989). In this case, the matrix  $S_v$  in (2.41) becomes a square invertable matrix. Thus, it can be eliminated from the test statistic (2.43), which results in

$$T_G^f = v^T Q_v^{-1} v = \sum_{i=1}^{1+n} v_i^T Q_{v_i}^{-1} v_i \sim \chi^2(\sum_{i=1}^{1+n} m_i, 0) \quad \text{under } H_0 \quad . \quad (2.51)$$

Equation (2.51) is basically a *failure or alarm test* that tells us whether there is anything wrong in the system or not. If  $n = 0$  in (2.51), i.e. only the current one epoch innovations are used, it is called a Local failure or Local alarm test, which has the form:

$$T_G^{L-f} = v_{v_i}^T Q_{v_i}^{-1} v_i \sim \chi^2(m_i, 0) \quad \text{under } H_0 \quad . \quad (2.52)$$

Once the failure test (2.51) or (2.52) signifies a failure present in the system, the diagnosis of the failure sources, i.e. bias identification or isolation process, is conducted. For this purpose, an approach similar to data-snooping (Baarda,1968) is employed in this research. That is, each individual postulated bias source is tested separately until all the possible bias sources are examined. This corresponds to the case when the dimension of the bias vector  $\mathbf{b}$  in (2.40) is chosen equal to one at each time. Thus the test statistic (2.43) reduces to a one-dimensional *identification or slippage* test (Teunissen and Salzmann, 1989):

$$t_g = \frac{(\sum_{i=1}^{1+n} s_i^T Q_{v_i}^{-1} v_i)^2}{\sum_{i=1}^{1+n} s_i^T Q_{v_i}^{-1} s_i} \sim \chi^2(1,0) \quad \text{under } H_0 \quad , \quad (2.53)$$

where  $s_i$  is a one dimensional vector and computed by equation (2.23). For instance, if one suspects sensor failures or outliers in the Kalman filter measurement model, one can choose  $C_k$  in (2.11) or (2.23) as

$$C_k^j = (0, \dots, 0, 1, 0, \dots, 0)^T \quad (2.54)$$

1                      j                       $m_k$

for  $j = 1, 2, \dots, m_k$ . This means that each observation is tested in turn to search biases.

If  $n$  is set to zero in (2.53), i.e. only the current epoch innovations are used for bias identification, it is called a Local identification and has the form:

$$t_g^L = \frac{(s_i^T Q_{v_i}^{-1} v_i)^2}{s_i^T Q_{v_i}^{-1} s_i} \sim \chi^2(1, 0) \quad \text{under } H_0 \quad (2.55)$$

Research experiences (Lu and Lachapelle, 1990; Wei et al, 1990) have shown that the local failure test (2.52) and the local identification test (2.55) are suitable for bias detection and identification in differential kinematic GPS surveying, since the most common and severe biases are cycle slips which are multiples of the carrier wavelength (19.02 cm). Therefore, the local test statistics (2.52) and (2.55) are used in the developed testing procedures.

Unfortunately in some cases, especially in large or multiple bias situations, the identification test (2.55) is too sensitive and may lead to many false bias alarms, signifying more biases than there are actually present. To overcome or alleviate this problem, a *new step* is introduced in the testing procedure by using the concept of minimum detectable bias (MDB). That is, for a bias signified by (2.55), its estimation value is compared against its corresponding MDB value. If the estimated value of the bias is larger than its corresponding MDB value, then this bias is considered an actual bias present in the Kalman filter models, otherwise it is considered as a false bias alarm and eliminated from the bias vector  $\mathbf{b}$ . By using this method, only the biases with more than the detection power  $1-\beta_0$  are retained and estimated.

Summarizing the above discussions, we arrive at the following testing procedures as depicted in Figure 2.2, which can be executed in parallel with the real-time Kalman filter algorithm.

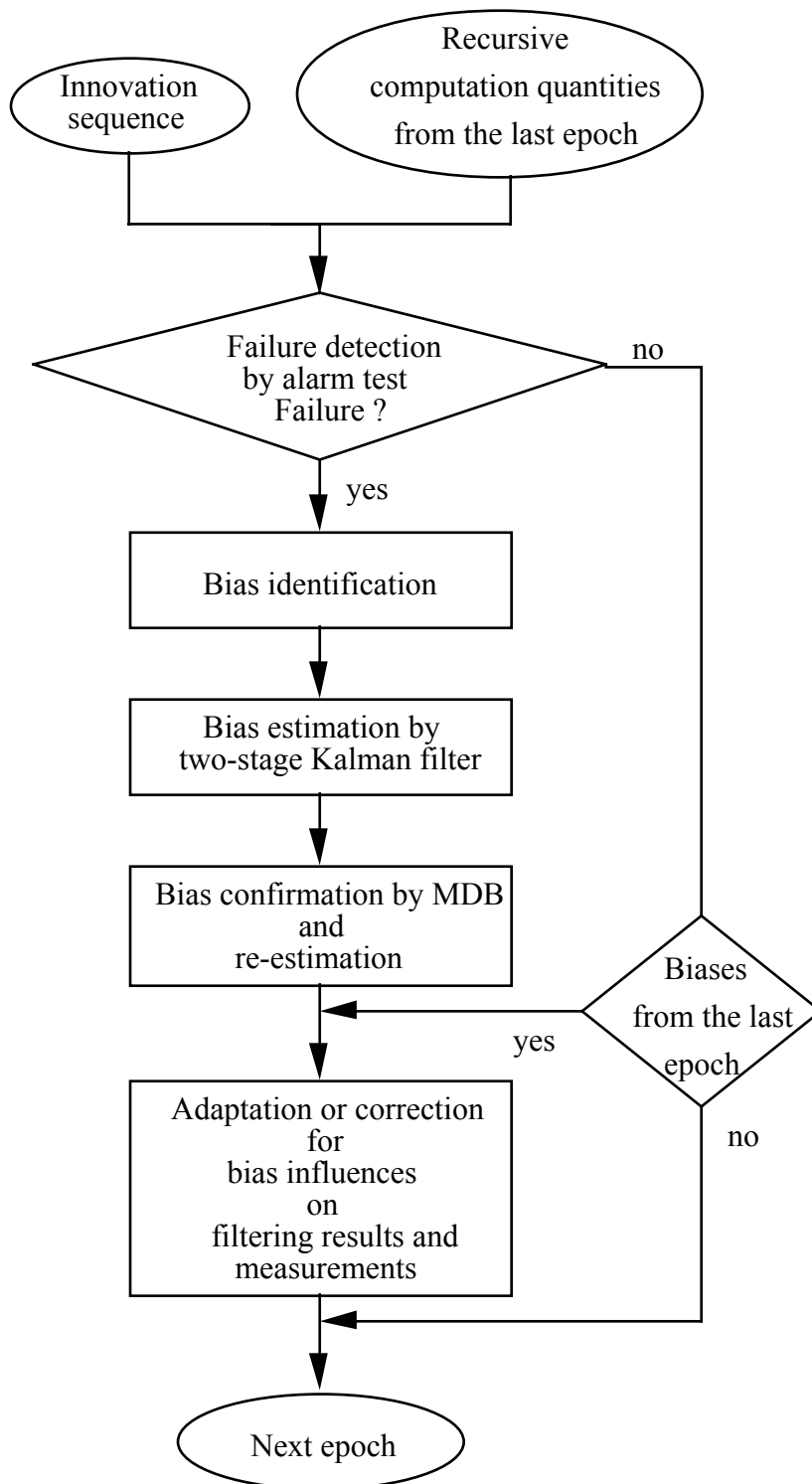


Fig. 2.2 Flowchart of the Testing Procedure for Use in Kalman Filters

CHAPTER 3

**KINEMATIC DIFFERENTIAL GPS POSITION AND  
VELOCITY ESTIMATION MODEL**

Generally speaking, there are two kinds of models used for combined processing of pseudo-range, carrier phase and Doppler frequency (phase rate) observations in precise kinematic differential GPS (DGPS) surveys. One is the *complementary filter* or *batch-solution* (Seeber et al, 1986; Hwang and Brown , 1990), in which one type of observable (e.g. pseudorange) is used for correcting the positions derived by another type of observable (e.g. carrier phase). The advantage of this type of modelling is that it does not require assumptions on the motion behaviour of the moving platform. However, this type of model cannot directly output the velocity and acceleration estimates. The second type of model is the *integrated filter* or *state space Kalman filter model* (Schwarz et al, 1989; Hwang and Brown, 1990), in which all available observations are processed simultaneously through a Kalman filter that describes the kinematic surveying system. This type of model has been widely tested under different environments and has yielded very good position and velocity estimation results in kinematic and semi-kinematic surveying (Schwarz et al, 1989; Cannon et al, 1990; Cannon, 1990; Cannon, 1991). Therefore, the integrated filter or state space Kalman filter model is used in this research for kinematic GPS data processing.

### 3.1 SYSTEM MODELS

In kinematic GPS surveying, if the satellite positions are considered fixed, the status of a moving vehicle can be described by the vehicle's position, velocity and acceleration in three-dimensional space, through the use of kinematic motion equations in physics (Schwarz et al, 1989). Usually, the *constant velocity* or *constant acceleration* model is adopted in surveying practice. The adequacy and accuracy of these models depends on the dynamics of the vehicle motion and the measurement update interval  $\Delta t$ . A detailed investigation and comparison of the model behaviours is given in Schwarz et al (1989). Experiences in this research show that a one second or higher data output rate is preferred for bias detection purposes when the constant velocity model or the constant acceleration model is used as the system model for land vehicle kinematic surveying systems. With the improvement of GPS receiver technology, most of the new receivers, such as, the department's Ashtech LD-XII, have a one Hz or higher data output rate. With such a short time interval between epochs, the constant velocity model or the constant acceleration model seems accurate enough for most of the kinematic land surveying tasks.

#### 3.1.1 Constant Velocity Model

Using the satellite-receiver double difference observables of the GPS system as the update measurements, the constant velocity model describing the vehicle motion consists of three position states ( $\delta\phi$ ,  $\delta\lambda$ ,  $\delta h$ ) and three velocity states ( $\delta v_n$ ,  $\delta v_e$ ,  $\delta v_h$ ). Thus, the state vector  $x_6$  of the constant velocity model reads

$$x_6 = ( \delta\phi, \delta\lambda, \delta h, \delta v_n, \delta v_e, \delta v_h )^T, \quad (3.1)$$

where  $\phi$  is the latitude,  $\lambda$  the longitude,  $h$  the height,  $v_n$  the north velocity,  $v_e$  the east velocity, and  $v_h$  the up velocity. Here we assume that before the kinematic run begins, the carrier phase ambiguity parameters have been resolved correctly by some common method, such as antenna swapping or occupying the initial baseline for about 10~15 minutes to allow for a static solution. Therefore, the ambiguity parameters are held fixed and do not appear in the state vector.

The states  $\delta v_n$ ,  $\delta v_e$ ,  $\delta v_h$  in (3.1) can be assumed to behave as a random walk or a first-order Gauss-Markov process, according to the vehicle motion. If the first-order Gauss-Markov process is used to describe the behaviour of the three velocity states, the transition matrix  $\Phi_{x_6}$  of the state vector  $x_6$  has the form:

$$\Phi_{x_6}(\Delta t) = \begin{pmatrix} \mathbf{I} & \mathbf{CD} \\ \mathbf{0} & \mathbf{T} \end{pmatrix}, \quad (3.2)$$

where all submatrices are diagonal and of dimension (3x3), which can be expressed as:

$$\mathbf{C}(\Delta t)_{3 \times 3} = \text{diag}(c_i) \quad \text{with} \quad c_i = \frac{1}{\alpha_i} (1 - \exp(-\alpha_i \Delta t)), \quad (3.3)$$

$$\mathbf{T}(\Delta t)_{3 \times 3} = \text{diag}(t_i) \quad \text{with} \quad t_i = \exp(-\alpha_i \Delta t), \quad (3.4)$$

$$\mathbf{D}_{3 \times 3} = \text{diag}(1/R, 1/R \cos\phi, 1). \quad (3.5)$$

where  $\alpha_i$  is the inverse of the correlation time of the stochastic Markov process,  $\Delta t$  is the update interval and  $R$  is the earth radius.

The covariance matrix  $Q_k$  of the system process noise related to  $x_6$  can be computed by simple numerical integration when the spectral density matrix of the system noise  $Q(t)$  is specified (Gelb, 1974), i.e.

$$Q_k = \int_{\tau=0}^{\Delta t} \Phi_{x_6}(\tau) Q(\tau) \Phi_{x_6}^T(\tau) d\tau \quad (3.6)$$

In the constant velocity model,  $Q(t)$  usually has the form

$$Q(t) = \begin{pmatrix} \mathbf{0} & \mathbf{0} \\ \mathbf{0} & \mathbf{Q}_2(t) \end{pmatrix}, \quad (3.7)$$

where  $\mathbf{Q}_2(t) = \text{diag}(q_{v_n}(t), q_{v_e}(t), q_{v_h}(t))$  are spectral densities of the three velocity states.

### 3.1.2 Constant Acceleration Model

Similar to the constant velocity modelling of the vehicle motion, the constant acceleration model uses the position states  $(\delta\phi, \delta\lambda, \delta h)$ , velocity states  $(\delta v_n, \delta v_e, \delta v_h)$  and acceleration states  $(\delta a_n, \delta a_e, \delta a_h)$  to describe the motion of the vehicle in 3-dimensional space. This leads to the following filter state vector

$$x_9 = (\delta\phi, \delta\lambda, \delta h, \delta v_n, \delta v_e, \delta v_h, \delta a_n, \delta a_e, \delta a_h)^T, \quad (3.8)$$

where the three additional acceleration states  $\delta a_n, \delta a_e, \delta a_h$ , corresponding to north, east and up accelerations respectively, are added. In this model, the three acceleration states are considered to be driven by Gaussian noise and to behave as a random walk or a Gauss-Markov process depending on the vehicle dynamics. If the first-order Gaussian-Markov process is used to describe the acceleration states, the transition matrix of state vector (3.8) reads

$$\Phi_{x_9}(\Delta t) = \begin{pmatrix} \mathbf{I} & \mathbf{D}\Delta t & \mathbf{FD} \\ \mathbf{0} & \mathbf{I} & \mathbf{C} \\ \mathbf{0} & \mathbf{0} & \mathbf{T} \end{pmatrix}, \quad (3.9)$$

where submatrices  $\mathbf{C}$ ,  $\mathbf{T}$  and  $\mathbf{D}$  are defined as in (3.3), (3.4) and (3.5). The submatrix  $\mathbf{F}$  has the form

$$\mathbf{F}(\Delta t)_{3 \times 3} = \text{diag}(f_i) \quad \text{with } f_i = \frac{1}{\alpha_i^2}(\exp(-\alpha_i \Delta t) + \alpha_i \Delta t - 1). \quad (3.10)$$

The covariance matrix of the system noise is computed by simple numerical integration

$$\mathbf{Q}_k = \int_{\tau=0}^{\Delta t} \Phi_{x_0}(\tau) \mathbf{Q}(\tau) \Phi_{x_0}^T(\tau) d\tau \quad (3.11)$$

with the spectral densities

$$\mathbf{Q}(t) = \begin{pmatrix} \mathbf{0} & \mathbf{0} & \mathbf{0} \\ \mathbf{0} & \mathbf{0} & \mathbf{0} \\ \mathbf{0} & \mathbf{0} & \mathbf{Q}_3(t) \end{pmatrix}, \quad (3.12)$$

where  $\mathbf{Q}_3(t) = \text{diag}(q_{a_n}(t), q_{a_e}(t), q_{a_h}(t))$  are spectral densities of the three acceleration states.

The models described above are similar to those in Schwarz et al (1989) with one difference. In Schwarz et al (1989), a carrier phase cycle slip is treated as a random state and estimated by the augmented Kalman filter algorithm, whereas in our approach, a cycle slip occurring on a satellite is treated as a constant bias to be recursively estimated and corrected by a two-stage Kalman filter.

### 3.2 OBSERVATION MODEL

Observations are used for updating and correcting the Kalman filter states predicted by the system model. Basically, the GPS system provides two fundamental observables for geodetic surveying purposes. They are the code pseudo-range observable and the carrier phase

observable. For most of the navigation/geodetic GPS receivers, another type of observable, the instantaneous phase rate (Doppler frequency) is also output for instantaneous velocity determination of the moving vehicle.

The basic observation equation for raw pseudorange observations,  $p$ , is (Lachapelle, 1990):

$$p = \rho + c(dt - dT) + d\rho + d_{ion} + d_{trop} + \varepsilon(p) \quad (3.13)$$

where  $\rho$  is the geometric range between the receiver antenna and a satellite,

$c$  is the speed of light,

$dt, dT$  are the satellite and receiver clock errors respectively,

$d\rho$  is the range error resulted from satellite orbital errors,

$d_{ion}, d_{trop}$  are the ionospheric and tropospheric corrections, respectively,

and  $\varepsilon(p)$  is the pseudo-range measurement noise.

The pseudorange measurements are instantaneous and unambiguous, but their high measurement noise level limits their use in practice for precise positioning. The typical measurement noise of pseudoranges is in the order of 1 to 4 metres for C/A code and within the submetre level for P code. Furthermore, pseudo-range observables are vulnerable to multipath influences which can often result in errors up to 20 m level in C/A code measurements (Lachapelle, 1990).

The observation equation for raw carrier phase observations,  $\Phi$ , is (Wells et al, 1986; Lachapelle, 1990)

$$\Phi = \rho + c(dt - dT) + \lambda N + d\rho - d_{ion} + d_{trop} + \varepsilon(\Phi) \quad (3.14)$$

where  $\Phi = -\lambda\phi_{\text{measured cycles}}$  ( $\Phi$  in meters),

$N$  is the initial carrier phase cycle ambiguity,

$\varepsilon(\Phi)$  is the carrier phase measurement noise,

and  $\lambda$  is the wavelength of the carrier signal (metre).

The main advantages of the carrier phase observable are its low measurement noise level (usually about 2 mm) and its low sensitivity to multipath effects (usually not exceeding  $0.25\lambda$ ). But, in order to use carrier phase observables to obtain precise and reliable kinematic positioning results, the initial carrier phase ambiguity  $N$  should be correctly resolved before kinematic data collection begins. Also, the lock on carrier signals of the satellites should be maintained during data collection unless the cycle slip problem can be effectively solved by some methods or external sources. A cycle slip is a discontinuity in the received carrier phase observations, which results in a change in the integer ambiguity  $N$ .

Phase rate or Doppler frequency is the time derivative of the phase. The observation equation of phase rate can be expressed as:

$$\dot{\Phi} = \dot{\rho} + c(\dot{dt} - \dot{dT}) + \dot{d}\rho - \dot{d}_{\text{ion}} + \dot{d}_{\text{trop}} + \dot{\varepsilon}(\Phi) \quad (3.15)$$

where  $(\dot{\quad})$  denotes the derivative with respect to time. The linearized form of (3.15) in the geodetic coordinate system  $(\phi, \lambda, h)$  is given by (Lu et al, 1990)

$$\begin{aligned} \delta\dot{\Phi} = & \left(a \frac{\partial x}{\partial \phi} + b \frac{\partial y}{\partial \phi} + c \frac{\partial z}{\partial \phi}\right) \delta\phi + \left(a \frac{\partial x}{\partial \lambda} + b \frac{\partial y}{\partial \lambda} + c \frac{\partial z}{\partial \lambda}\right) \delta\lambda + \left(a \frac{\partial x}{\partial h} + b \frac{\partial y}{\partial h} + c \frac{\partial z}{\partial h}\right) \delta h \\ & + \frac{\partial \rho \delta V_n}{\partial \phi R} + \frac{\partial \rho \delta V_e}{\partial \lambda R \cos \phi} + \frac{\partial \rho}{\partial h} \delta V_h + c(\delta\dot{dt} - \delta\dot{dT}) + \dot{d}\rho - \dot{d}_{\text{ion}} + \dot{d}_{\text{trop}} + \dot{\varepsilon}(\Phi) \quad , \end{aligned} \quad (3.16)$$

where

$$a = \frac{\partial^2 \rho}{\partial x^2} (\dot{x}_R - \dot{x}_r) + \frac{\partial^2 \rho}{\partial x \partial y} (\dot{y}_R - \dot{y}_r) + \frac{\partial^2 \rho}{\partial x \partial z} (\dot{z}_R - \dot{z}_r)$$

$$b = \frac{\partial^2 \rho}{\partial y \partial x} (\dot{x}_R - \dot{x}_r) + \frac{\partial^2 \rho}{\partial y^2} (\dot{y}_R - \dot{y}_r) + \frac{\partial^2 \rho}{\partial y \partial z} (\dot{z}_R - \dot{z}_r)$$

$$c = \frac{\partial^2 \rho}{\partial z \partial x} (\dot{x}_R - \dot{x}_r) + \frac{\partial^2 \rho}{\partial z \partial y} (\dot{y}_R - \dot{y}_r) + \frac{\partial^2 \rho}{\partial z^2} (\dot{z}_R - \dot{z}_r) \quad .$$

The above raw observables are severely affected by different error sources, such as orbital errors, satellite clock and receiver clock errors and atmospheric errors. One effective way to eliminate or reduce these error terms is to form the differenced observables from the raw ones. Differencing of simultaneous observations usually cancels the common error terms. In GPS data processing, the widely used differencing modes are the single difference(SD), double difference(DD) and triple difference(TD) (Remondi, 1984; Wells et al, 1986). In this research, the (receiver-satellite) double difference (DD) observables of pseudo-range, carrier phase and phase rate are used as the measurement updates in the Kalman filter for kinematic GPS position and velocity estimation. Thus, the observation model reads:

$$\nabla \Delta p = \nabla \Delta \rho + \nabla \Delta d_{\text{ion}} + \nabla \Delta d_{\text{trop}} + \nabla \Delta \epsilon(p) \quad (3.17)$$

$$\nabla \Delta \Phi = \nabla \Delta \rho + \lambda \nabla \Delta N + \nabla \Delta d_{\text{ion}} + \nabla \Delta d_{\text{trop}} + \nabla \Delta \epsilon(\Phi) \quad (3.18)$$

$$\nabla \Delta \dot{\Phi} = \nabla \Delta \dot{\rho} - \nabla \Delta \dot{d}_{\text{ion}} + \nabla \Delta \dot{d}_{\text{trop}} + \nabla \Delta \dot{\epsilon}(\Phi) \quad (3.19)$$

where  $\nabla \Delta$  is the double difference operator between two stations and two satellites (Wells et al, 1986).

It is noted that double difference observations cancel out the satellite clock errors and receiver clock errors, and reduce the orbital and atmospheric errors. Another advantage of the double difference GPS observable is that the integer nature of cycle ambiguity  $\nabla \Delta N$  in (3.18)

can be exploited. Once the integer ambiguity is resolved, it can be held fixed in kinematic surveys. Unfortunately, if cycle slips occur in carrier phase observations, which is often the case in real kinematic surveys, the phase measurement update equation (3.18) is no longer valid but biased by a constant value, which in turn results in erroneous position and velocity estimates in the filter. Therefore, it is necessary to have some ways to check and correct cycle slips in the observation model. And this is one of the main problems to be dealt with in the quality control of precise kinematic GPS surveying.

CHAPTER 4  
**RELIABILITY ANALYSIS IN KINEMATIC  
DIFFERENTIAL GPS SURVEYS**

Reliability analysis in kinematic GPS surveys includes two aspects, the minimum detectable bias (MDB) in the filter models and the influences of the undetectable bias on the filtering results. In this Chapter, the bias influence characteristics on position and velocity estimation are investigated and the MDB values of some common biases in kinematic GPS surveys are examined. All these analyses can be done prior to the actual survey campaign, based on the theoretical formulas given in Chapter 2 and the assumed surveying conditions. Familiarity with the bias influence behaviors and the MDB values of some common biases as well as their correlation with the satellite number and satellite geometry is very helpful in the planning stage of kinematic GPS surveying.

**4.1 BIAS INFLUENCES ON POSITION AND VELOCITY ESTIMATION IN  
KINEMATIC DIFFERENTIAL GPS SURVEYS**

This section investigates the theoretical influences of different kinds of biases on the position and velocity estimation by using two-stage Kalman filter formulation. In kinematic GPS surveys, the most common biases in the observation (double difference) model are cycle

slips in carrier phases, outliers in pseudoranges and outliers in phase rates. The likely biases when using the system model are the acceleration errors in the constant velocity model and the acceleration disturbances in the constant acceleration model. In the following sub-sections, the bias influence for each kind of bias is developed. The total influence of biases are then the *summation* of the influences of each kind of bias, since the bias influences on Kalman filtering results are linear in nature. These theoretical bias influences, based on the adopted models and *assumed* surveying environments, lead to a better understanding of the problems and concerns in kinematic GPS positioning.

In order to inter-compare the magnitude of the different bias influences on position states and velocity states, we define a scalar term as follows:

**Local Bias-to-Noise Ratio in states (LBNR)** is the ratio between the bias  $\nabla x_i$  in a given Kalman state  $x_i$ , caused by a bias vector  $\mathbf{b}$ , and its standard deviation  $\sigma_{x_i}$ , i.e. 
$$\text{LBNR} = \nabla x_i / \sigma_{x_i} .$$

In the following computations, we used a part of the trajectory of the semi-kinematic GPS surveying run carried out in Kananaskis Country on Julian day 222, 1990. This part of the trajectory consisted of 59 epochs (4 minutes duration) and started at 494132 seconds. Six satellites were available above an elevation angle of  $15^0$  in this part of trajectory. The dilutions of precision for latitude, longitude and height within the adopted trajectory are given in Figure 4.1. The height dilution of precision is good but relatively poorer than the latitude and longitude dilutions of precision. The maximum speed of the vehicle reached 80km/h. The standard deviations assumed for the pseudorange, carrier phase and phase rate observations were 4 m, 2 cm and  $5 \text{ cm s}^{-1}$ . The output data rate was 4 seconds. All the computations were done using the program package QUALIKIN described in Chapter 6 and the constant velocity model was employed as the system model of the Kalman filter for bias influence analysis.

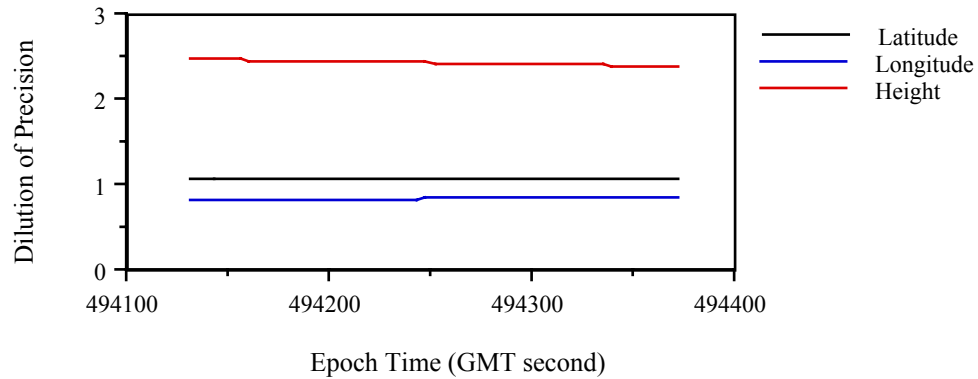


Fig. 4.1 Dilution of Precision for Part of the Trajectory of Day 222, 1990

**(a) Influences of Cycle Slips in Carrier Phase Observations**

In double difference (receiver-satellite) carrier phase observations, cycle slips can be modelled as constant biases following the epoch at which they occur. Figure 4.2 shows one example of the influence of carrier phase cycle slips on the estimated positions and velocities. Here we assume that one cycle slip 19.02 cm occurs on SV 11 starting from 494132 seconds. The pseudorange and phase rate observations as well as the system model are assumed bias-free. In Figure 4.2,  $\nabla\phi$ ,  $\nabla\lambda$  and  $\nabla h$  denote the scalar errors (LBNR) in latitude, longitude and height respectively, caused by the assumed one cycle slip.  $\nabla V_n$ ,  $\nabla V_e$  and  $\nabla V_h$  are the scalar errors (LBNR) in north velocity, east velocity and up velocity, respectively. Figure 4.3 shows another example where two satellites, instead of one, are assumed to have cycle slips.

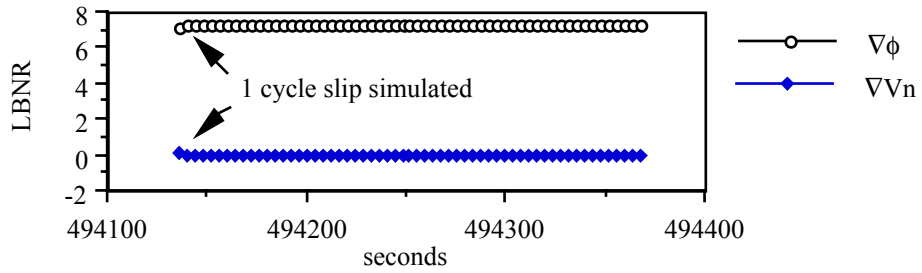


Fig. 4.2(a) LBNR for latitude and Vn

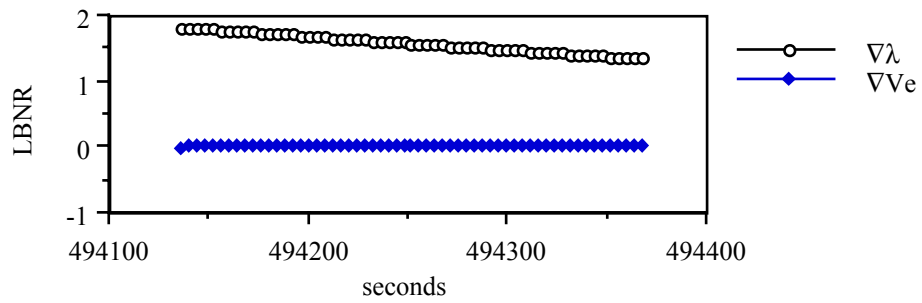


Fig. 4.2(b) LBNR for longitude and Ve

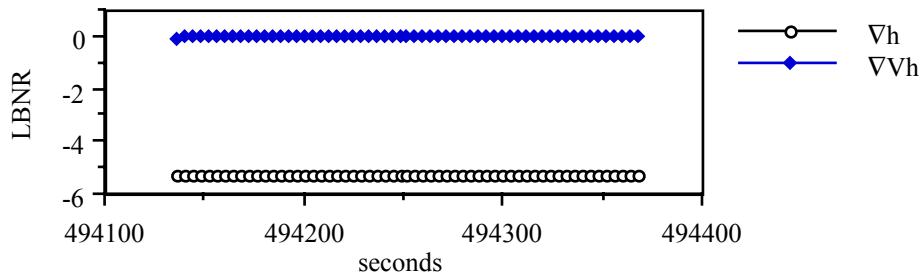


Fig. 4.2(c) LBNR for height and Vh

Fig. 4.2 Cycle slips influences on positions and velocities. Six satellites (SVs 2,6,9,11,13,18 ) are available simultaneously. SV 11 is assumed to have one cycle slip (19.02cm) starting from 494132 seconds. The data interval is 4 seconds.

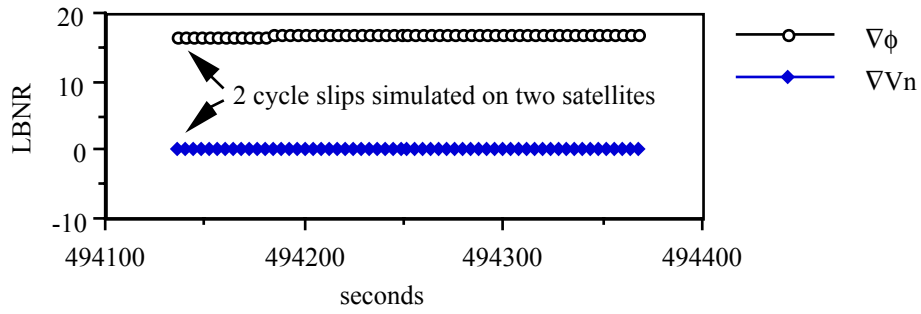


Fig. 4.3(a) LBNR for latitude and Vn

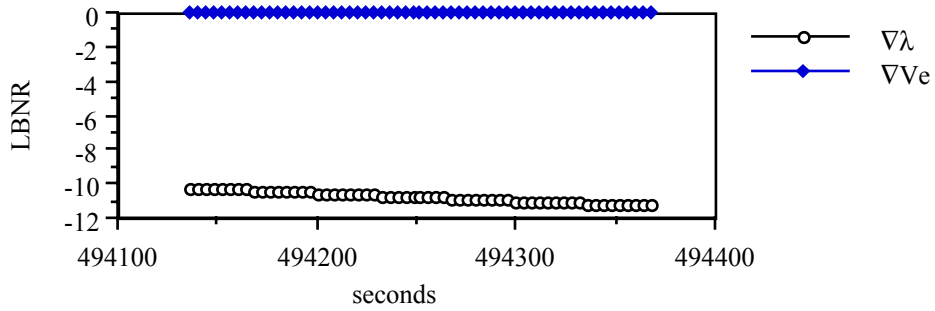


Fig. 4.3(b) LBNR for longitude and Ve

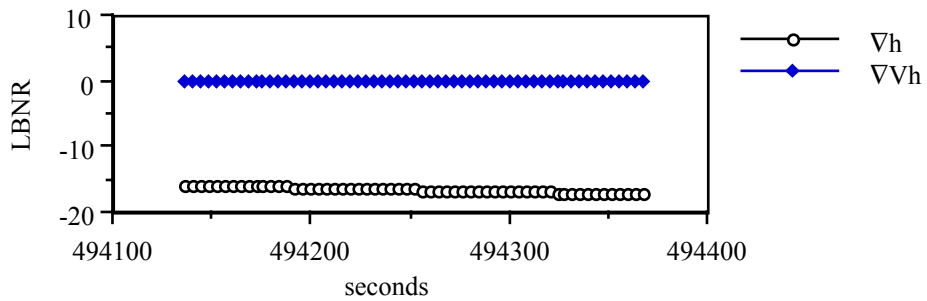


Fig. 4.3(c) LBNR for height and Vh

Fig. 4.3 Cycle slip influences on positions and velocities. Six satellites (SVs 2,6,9,11,13,18 ) are available simultaneously. Two satellites (SVs 11,18) are assumed to have two cycles slip starting from 494132 seconds. The data interval is 4 seconds.

From the above examples, we note that carrier phase cycle slips mostly affect the estimated positions as opposed to the estimated instantaneous velocities. For one cycle slip occurring on one satellite, the maximum influence on latitude estimates, as shown in Fig. 4.2(a), reached about 8 times their standard deviations, or about 10 cm in absolute magnitude. The more satellites affected by cycle slips, the more severe the influences. The total influences of multiple cycle slips are the summation of the individual cycle slip influence because of the linear property of the bias effects on the Kalman filtering results. Figures 4.2 and 4.3 also show that the cycle slips have a permanent or long-term effect on the estimated positions. Their influences on the estimated positions are not constant but slowly drifting in time with the changing satellite geometry. Since the time span in these examples was short (4 minutes), the drift effect was not very significant. Cannon (1991) has shown one example in which the drift in height component reached about 14 cm for a one hour duration, when one cycle slip was introduced in the carrier phase observations. Therefore, real-time correction and adaptation of the cycle slips in double difference observations are important to assure the correctness of the kinematic positioning results.

#### **(b) Influences of Outliers in Pseudorange Observations**

We define an outlier herein as an instantaneous bias that only affects the epoch at which it occurs. Fig. 4.4 shows the influence of a pseudorange outlier of 20 m on SV 9 at 494132 seconds where six satellites were in view and the vehicle was moving at a speed of  $36 \text{ km h}^{-1}$ .

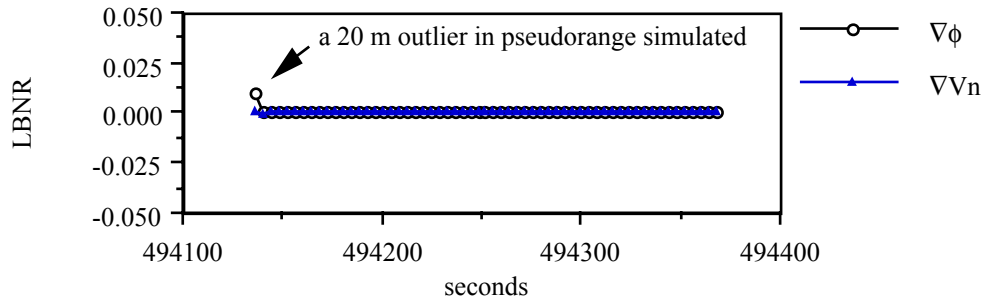


Fig. 4.4(a) LBNR for latitude and  $V_n$

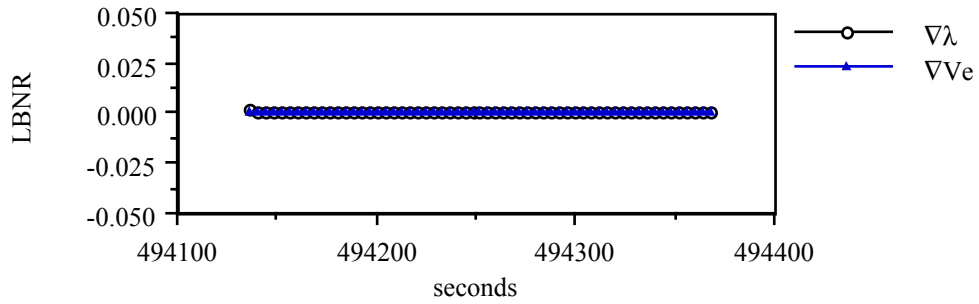


Fig. 4.4(b) LBNR for longitude and  $V_e$

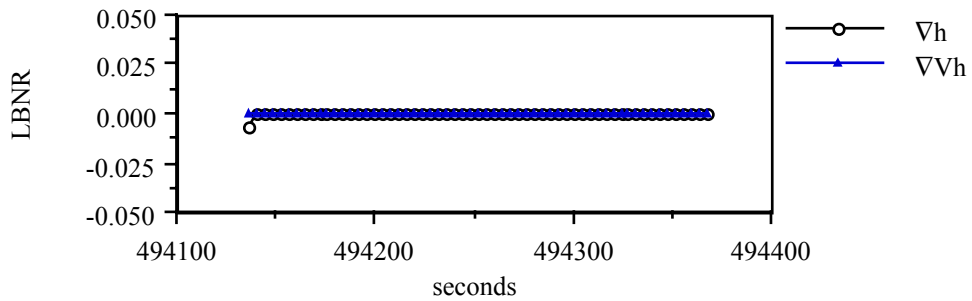


Fig. 4.4(c) LBNR for height and  $V_h$

Fig. 4.4 Pseudorange outlier influences on positions and velocities. Six satellites (SVs 2,6,9,11,13,18) are in view simultaneously. A single outlier of 20 m is assumed in the pseudorange of SV 11 at 494132 seconds. The data interval is 4 seconds.

From the single outlier case shown in Fig. 4.4 and other test computations, we notice that the magnitude (LBNR) of the influences of pseudorange outliers on positions and velocities is much smaller than that due to cycle slips and practically can be neglected. This is caused by the lower a priori standard deviation of pseudorange observations. The pseudorange outliers mainly affect the positions as opposed to the velocities. Furthermore, such effects are only limited to the current and subsequent few epochs when no bias occurs on the phase and phase rate measurements. This means that the Kalman filter can reduce the outlier influence on the estimated states after a few epochs of measurement updates. Here we assume that the system model is correct.

**(c) Influences of Outliers in Phase Rate Observations**

Unlike the carrier phase observation which is the accumulated cycles of the received carrier signal, phase rate (Doppler) is an instantaneous observation that reflects the changing range rate from the receiver to the observed satellite. The likely biases in phase rate observations are outliers present on each single measurement. Fig. 4.5 shows the influences on the estimated positions and velocities for an outlier of  $0.5\text{ m s}^{-1}$  occurring at time 494132 in the phase rate observation of SV 11.

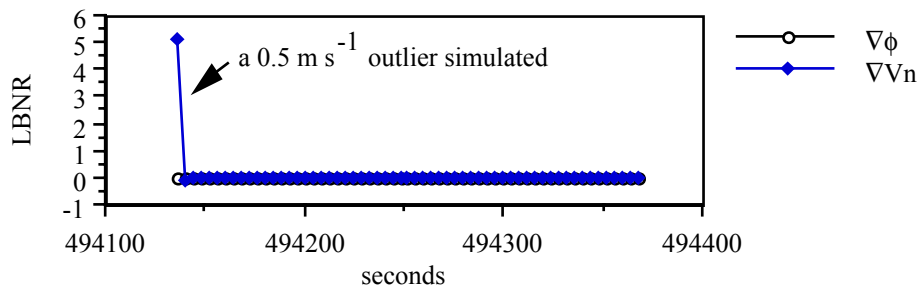


Fig. 4.5(a) LBNR for latitude and  $V_n$

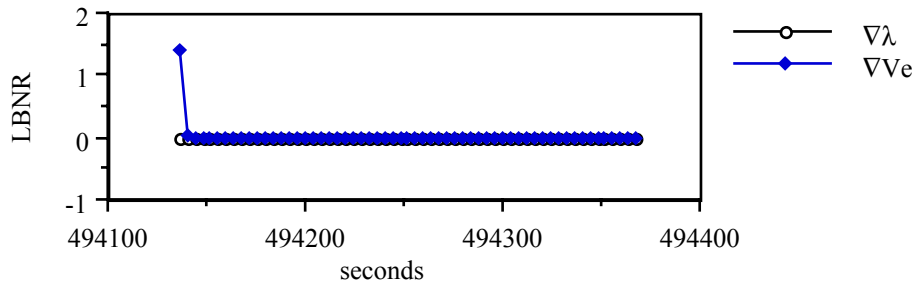


Fig. 4.5(b) LBNR for longitude and  $V_e$

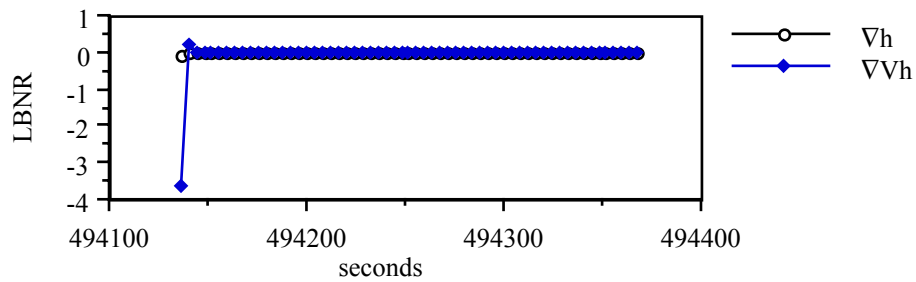


Fig. 4.5(c) LBNR for height and  $V_h$

Fig. 4.5 Phase rate outlier influences on positions and velocities. Six satellites (SVs 2,6,9,11,13,18) are available simultaneously. A single outlier of  $0.5\text{m s}^{-1}$  in the phase rate occurs on SV 11 at 494132 seconds. The data interval is 4 seconds.

We note two points from Figure 4.5. Firstly, the outlier in phase rate observations mainly affects the estimated velocities. This is different from the cycle slip influences which mainly affect the estimated positions. Secondly, the phase rate outlier influences on velocities are limited to the epoch at which the outlier occurs and the following few epochs. The Kalman filter can effectively reduce the outlier influences on the filtering states after a few epochs of observation updates. This is due to the nature of an outlier, which, by its definition, only affects one observation at a single epoch.

**(d) Influences of the Bias in the System Kinematic Model**

Besides the biases in the observation model, biases in the system model may exist due to deviations between the assumed and the actual vehicle motion. According to the Kalman filter algorithm, system model biases mainly affect the prediction or time propagation of the filter state vector  $\hat{x}_k(-)$ , which in turn influences the computation of the innovation sequence or predicted residuals. If the measurements are correct (bias-free), then the inaccurately predicted states  $\hat{x}_k(-)$  can be corrected by the measurement updates through the Kalman gain matrix  $K_k$ .

Fig. 4.6 shows one example of the system bias influences on the predicted states  $\hat{x}_k(-)$ , i.e. the predicted positions and velocities. Here we assume that within a constant velocity model (3.1), a single acceleration bias of  $2 \text{ m s}^{-2}$  occurs on the system state  $V_n$ , the main direction of the trajectory, for 6 consecutive epochs from time 494132 to 494152. The data rate is 4 seconds. The local bias-to-noise ratio (LBNR) in this example is defined by  $\nabla\phi(-)/\sigma_\phi(-)$ .

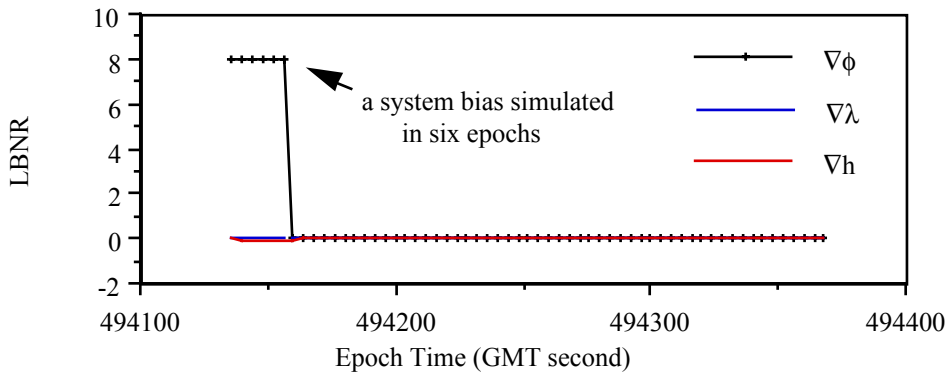


Fig. 4.6(a) LBNR for Latitude, Longitude and Height

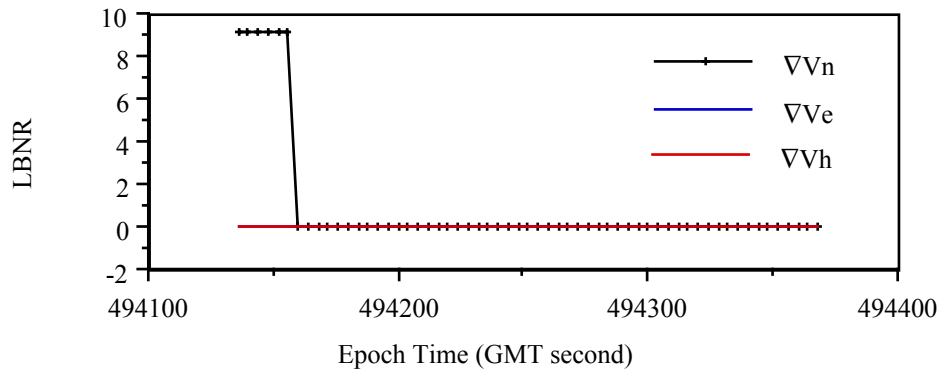


Fig. 4.6(b) LBNR for Northing, Easting and Up Velocities

Fig. 4.6 System bias influences on predicted positions and velocities. An acceleration bias of  $2 \text{ m s}^{-2}$  occurs on the system state  $V_n$  at 6 consecutive epochs from time 494132 to 494152. Six satellites (SVs 2,6,9,11,13,18) are available simultaneously. The data interval is 4 seconds.

From Fig. 4.6, one can see that the acceleration bias in the system model severely affects the corresponding *predicted* states  $\delta\Phi_k(-)$  and  $\delta V_n(-)$ . The absolute magnitudes of influences reach 16 metres in latitude and  $8 \text{ m s}^{-1}$  in northing velocity. These influences are limited to the epochs at which the system bias occurs. The shorter the update or data rate interval, the smaller the magnitude of influence. For instance, under the same conditions but at an update interval of 1 second, the magnitudes of influence reduce to 1 metre in latitude and  $1 \text{ m s}^{-1}$  in northing velocity. In order to limit the system bias influences on the innovation sequence and facilitate the detection of observation biases, a high data update rate (e.g. 1 second or higher), is recommended.

## 4.2 MDB IN KINEMATIC DIFFERENTIAL GPS SURVEYING MODEL

Minimum Detectable Bias (MDB) analysis is an important tool for Kalman filter design. It tells us about the filter's theoretical ability to detect the concerned biases under the assumed surveying conditions. Based on the formulas given in Section 2.3.1 of Chapter 2, the MDB values of some typical biases in the kinematic GPS position and velocity estimation models are investigated in this section. These biases include the carrier phase cycle slips, outliers in pseudoranges and outliers in phase rate measurements.

In all the following computations, the same trajectory from Julian Day 222, 1990 described in Section 4.1 was used. The non-centrality parameter for MDB computations is set to  $\lambda_0 = (4.13)^2$ , which corresponds to 0.1% and 20% probabilities of Type I and Type II errors, respectively, in a one-dimensional hypothesis test. Corresponding to the testing statistics and the testing procedure used in the bias detection and identification in kinematic GPS surveying, the *local MDB* (or the instantaneous MDB at each epoch) for a *single* bias case is of great importance, which, from equation (2.50), is given by

$$\mathbf{b}_{0i} = \sqrt{\frac{\lambda_0}{\mathbf{S}_i^T \mathbf{Q}_v^{-1} \mathbf{S}_i}}, \quad (4.1)$$

where  $i$  is the index for epochs. Here we define the *single* bias case as the case where no biases other than the specified one are presented in the processing models. The relationship between the local MDB values and the satellite geometry is also examined.

**(a) MDB for Carrier Phase Cycle Slips**

Cycle slips are common biases occurring during carrier phase measurements. They can be treated as constant biases in the receiver-satellite double difference observables if the initial carrier phase ambiguities are resolved and held fixed during the kinematic survey.

Fig. 4.7 shows the improvements in minimum detectable bias values at each epoch in double difference carrier phase observations of SV 02 with different satellite coverages. Fig. 4.8 shows the corresponding GDOP values of different satellite coverages. The four, five and six satellite coverages used for comparisons are (SVs 6, 2, 9, 11), (SVs 6, 2, 9, 11, 13) and (SVs 6, 2, 9, 11, 13, 18). Here we assume that only the concerned biases, i.e. cycle slips, are presented in the observations and the system model is errorless.

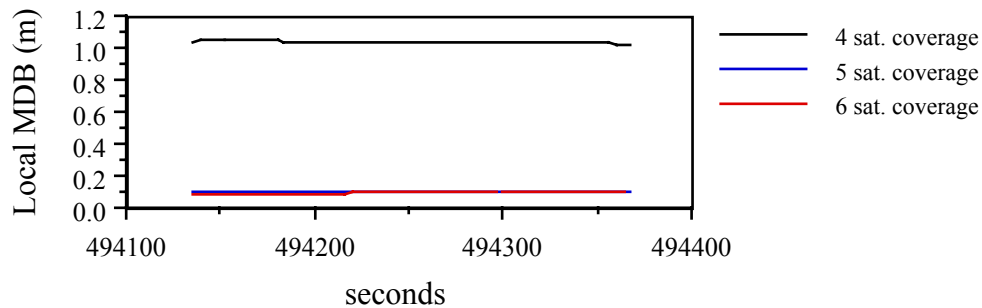


Fig. 4.7 Local MDB Improvement in Double Difference Carrier Phase Observations on SV 02 with the Different Satellite Coverages.

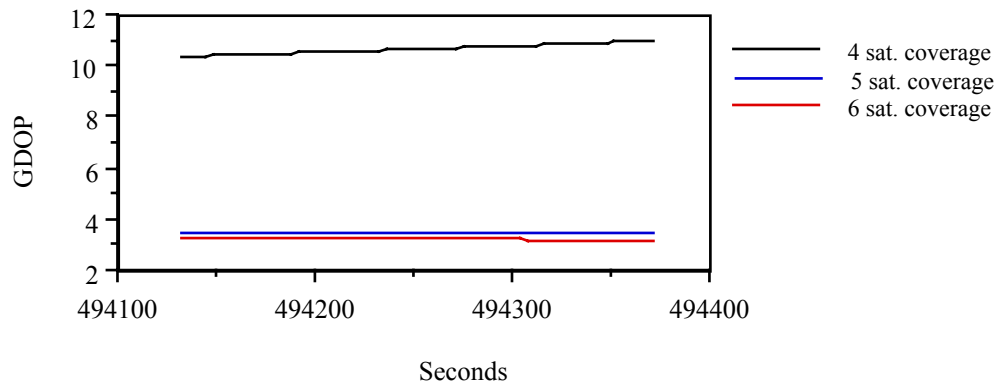


Fig. 4.8 GDOP improvements with the different satellite coverages

Figures 4.7 and 4.8 show that the MDB values at each epoch in the double difference carrier phase observations of SV 02 with the 4 satellite coverage, where the GDOP values reach approximately 10, are about 1 metre (i.e. 5 cycles of L1 frequency). With the 5 and 6 satellite coverages, where the GDOP values are around 3.2, the corresponding MDB values drop to about 0.1 metre (i.e. 0.5 cycle of L1 frequency). These MDB values reflect the best or theoretical values that the statistical testing can detect with a given testing power for a single bias present in the carrier phase observations, under the assumed surveying conditions. Comparing Fig. 4.7 with Fig. 4.8, we can see a correlation exists between the local (or instantaneous) MDB value and the satellite geometry. The stronger the geometry, the better the ability to detect a bias in the carrier phase observations. For reliable cycle slip detection on any individual satellite,  $GDOP \leq 4$  or coverage with five or more satellites is recommended.

**(b) MDB for Outliers in Phase Rate Observations**

An outlier can be modelled as an instantaneous bias appearing at a specific epoch. Outliers in phase rate measurements mainly affect the instantaneous velocity estimation. Fig. 4.9 shows the improvements in the minimum detectable outlier at each epoch in double

difference phase rate observations of SV 02 with the different satellite coverages. The GDOP values corresponding to each satellite coverage are the same as those shown in Fig. 4.8.

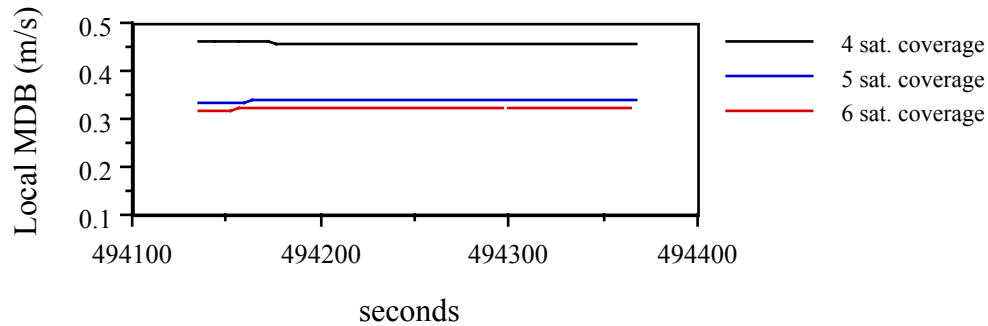


Fig. 4.9 Local MDB Improvements in Double Difference Phase Rate Observations on SV 02 with the Different Satellite Coverages.

It is noted that in the 4 satellite coverage, the minimum detectable outlier on SV 02 in phase rate observations at each epoch is about  $0.5 \text{ m s}^{-1}$ . If the available satellites increase to 5 or 6, the corresponding MDB values at each epoch for a single phase rate outlier drop to  $0.3 \text{ m s}^{-1}$ . This also means that the stronger the geometry, the better the detectability for phase rate outliers on each satellite.

**(c) MDB for Outliers in Pseudorange observations**

Pseudorange outlier detection is one of the main concerns of GPS integrity monitoring. Using the reliability analysis method given in this research, the minimum detectable pseudorange outlier can be easily obtained. The following example shows the local MDB value at each epoch for the single outlier case in the pseudoranges of SV 02.

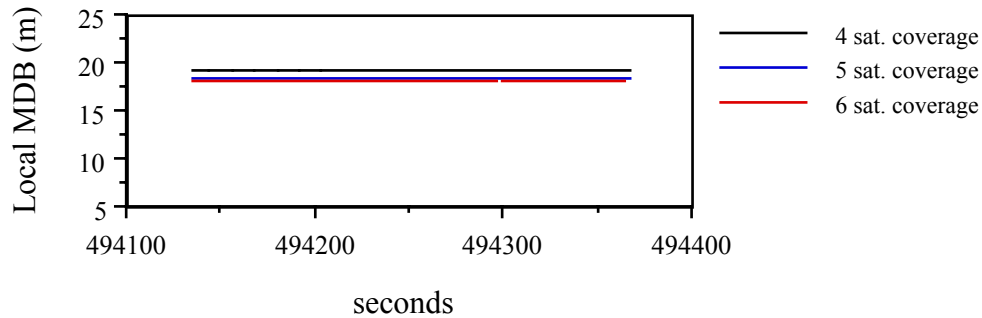


Fig. 4.10 Local MDB Improvements in Double Difference Pseudorange Observations on SV 02 with the Different Satellite Coverages.

Fig. 4.10 indicates that the minimum detectable pseudorange outlier at each epoch on SV 02 is about 18 m with the given testing parameters in the estimation filter. This means that if a single outlier occurs in the pseudoranges on SV 02, it can be detected with 80% probability only when this outlier is larger than 18 m. This value is approximately 4.5 times the pseudorange standard deviation. Furthermore, the MDB values does not improve much with the increase in the number of satellites. This is due to the much lower precision of the pseudoranges as compared to those of the carrier phase and phase rate observations in the filter.

The MDBs of the system biases can also be investigated as above. The numerical results are not given here. Generally, the minimum detectable acceleration bias in the constant velocity model, based on the trajectory and parameters given in Section 4.1, is about  $2 \text{ m s}^{-2}$ .

Summarizing the discussions in this Chapter, we conclude that reliability analysis is a useful tool in Kalman filter design. It is able to provide us some insights about the bias influence characteristics and the minimum detectable bias values for the concerned biases in the designed filters. Thus, a reliable filter operation scheme and a better understanding of the estimated results can be achieved.

CHAPTER 5

**CARRIER PHASE AMBIGUITY INITIALIZATION FOR  
DIFFERENTIAL KINEMATIC GPS SURVEYING**

In order to obtain cm-level accuracy with differential kinematic GPS positioning, the carrier phase ambiguities  $\nabla\Delta N$  in the measurement update eqn. (3.18) have to be resolved over the initial baseline before the vehicle goes into the kinematic mode and phase lock should be maintained on a minimum number of satellites thereafter (e.g. 4 satellites in a good geometry). However, during the period of kinematic GPS surveys, cycle slips on all or most of the available satellites may occur due to carrier signal obstruction by objects or other tracking problems. In such a situation, the initially resolved carrier phase ambiguities  $\nabla\Delta N$  of all the corresponding satellites, which are held fixed in equation (3.18), will change by an arbitrary integer number of cycles. Therefore, the new carrier phase ambiguities  $\nabla\Delta N$  of all or most of the satellites have to be resolved again or re-initialized during the kinematic surveying mode in order to maintain the cm-level positioning accuracy. This is a really difficult task that has not yet been fully solved. In this chapter, existing methods that have been currently used for carrier phase initialization in differential kinematic and semi-kinematic GPS data processing are discussed.

## 5.1 PHASE AMBIGUITY INITIALIZATION IN STATIC MODE

Carrier phase ambiguity initialization in static mode may be carried out at the beginning of a kinematic or semi-kinematic GPS surveying session to obtain the initial double difference phase ambiguities of each satellite. Once the initial phase ambiguities are resolved, they are held fixed and used as constant corrections to the carrier phase observables in the subsequent kinematic or semi-kinematic survey unless the ambiguities are affected by cycle slips. Currently, there are several ways used for the carrier phase initial ambiguity resolution in a kinematic or semi-kinematic survey. Among them are (1) surveying over a known baseline that has sufficient accuracy, (2) performing an antenna swapping manoeuvre (Hofmann-Wellenhof and Remondi, 1988), (3) occupying an initial unknown baseline sufficiently long to allow for a static solution of the initial baseline vector and the carrier phase ambiguities and (4) searching by the ambiguity function method (Remondi, 1990; Mader, 1990). All of these methods require that the initial baseline be relatively short to limit the orbital and atmospheric effects on the double difference observables. The fourth method, i.e. the ambiguity function method, can also be used in the phase ambiguity initialization in kinematic mode and therefore is discussed in the next section.

Surveying over a *known* initial baseline is the simplest method for initial phase ambiguity resolution. In this case, the initial baseline vector is held fixed and only the unknown ambiguity parameters  $\nabla\Delta N$  are solved for by using the collected static differential GPS phase data. The application of this method in practice, however, may be limited because we may not always have a known baseline available in the surveying area.

Antenna swapping is a time saving phase initialization method that does not require the a priori knowledge of the initial baseline. This method is well described in Hofmann-Wellenhof and Remondi (1988). Suppose that a pair of GPS receivers are placed at the two

ends of an initial baseline. After collecting GPS data for a few epochs, the two GPS receiver antennas are then swapped or exchanged and a few more epochs of observations are collected. During the process of antenna exchange and data collection, phase lock on at least 4 GPS satellites should be maintained. The effect of the swap is to produce a reversal of the satellite-receiver geometry while keeping the initial carrier phase ambiguities unchanged. By utilizing the information of the geometry change embodied in the data collected *before* and *after* antenna swapping, the initial baseline vector can be determined and hence the initial carrier phase ambiguities can be resolved. From the antenna swap procedures described above, we may note that the length of the initial baseline should be no more than a few metres in order to make the antenna swap easy and practical.

Occupying an initial baseline for a period sufficiently long to allow for a static batch least squares solution of the baseline vector and the initial phase ambiguities is the most widely used method for phase ambiguity initialization at the beginning of a kinematic or semi-kinematic GPS survey. This method can be applied to a baseline up to a few kilometres in length and also does not require the prior knowledge of the baseline except that one point of the baseline is held fixed and used as a master station for differential data processing. But we pay for these advantages with a *sufficiently long* static occupation time on the baseline, which is to allow for the satellites to "move appreciably" in order to accumulate sufficient geometry information for baseline vector and phase ambiguity determination. The required occupation time mainly depends on the satellite geometry and the carrier phase measurement noise, provided the atmospheric (ionospheric and tropospheric) effects can be neglected. In the field tests of this research with Ashtech LD-XII GPS receivers, 8 minutes of continuously static tracking data (4 second data rate) seemed sufficient to resolve the initial baseline vector and the initial phase ambiguities over a baseline less than 1 kilometre in length, when five or more satellites were available simultaneously with a GDOP value  $\leq 3.5$ . For reliable ambiguity

resolution for baselines up to a few kilometres in length, 10-30 minutes of static occupation is usually required.

## **5.2 PHASE AMBIGUITY INITIALIZATION IN KINEMATIC MODE**

When cycle slips are detected or present on all or most of the available satellites in kinematic mode and when the testing procedure together with the Kalman filter cannot resolve the correct integer ambiguities, some other carrier phase ambiguity initialization methods are then needed. Currently, there are several techniques used for the ambiguity resolution in kinematic GPS surveying or the "on the fly" ambiguity resolution. Among them are the extrawide-laning technique (Wubben, 1989), the least squares ambiguity search technique (Hatch, 1990) and the ambiguity function method (Counselman et al 1981; Remondi, 1984; Mader, 1990). Each of them has its own advantages and limitations. The extrawide-laning can be performed very quickly on individual satellites but it requires dual-frequency P-code GPS measurements. The least squares ambiguity search technique is a little faster computationally than the ambiguity function method (Hatch, 1990), but its theoretical foundation is not clear at this time and still under development. It requires more than 7 GPS satellites in view simultaneously for instantaneous ambiguity resolution. The ambiguity function method, on the other hand, is more involved computationally but has a good theoretical foundation and can be used in *static* mode or *kinematic* mode with multiple epochs of observations. For instantaneous ambiguity resolution in kinematic mode, it also requires 7 to 8 visible satellites (Mader, 1990). In this research, the ambiguity function method is tested and employed as an optional method for carrier phase ambiguity initialization in kinematic mode as well as in static mode.

### 5.2.1 Ambiguity Function Method (AFM)

The ambiguity function was first introduced by Counselman and Gourevitch (1981) and later by Remondi (1984) for static GPS carrier phase data processing. Its application in kinematic GPS surveying was recently discussed and tested by Mader (1990). Simply, the ambiguity function can be written as:

$$A(x, y, z) = \sum_{k=1}^K \left| \sum_{j=1}^{N-1} e^{i2\pi(\nabla\Delta\Phi^j(x_0, y_0, z_0)_{\text{obs}} - \nabla\Delta\Phi^j(x, y, z)_{\text{comp}})} \right|, \quad (5.1)$$

where  $K$  is the number of observation epochs,  $N$  the number of satellites at each epoch,  $|\cdot|$  is the norm operator,  $e^{i\theta}$  is the complex vector or phasor defined by  $e^{i\theta} = \cos\theta + i \sin\theta$ ,  $\nabla\Delta\Phi^j(x_0, y_0, z_0)_{\text{obs}}$  is the *observed* double difference observation in cycles at the correct position  $(x_0, y_0, z_0)$  and  $\nabla\Delta\Phi^j(x, y, z)_{\text{comp}}$  is the corresponding *computed* double difference observation in cycles at the trial position  $(x, y, z)$ .

An important characteristic of the phasor within the ambiguity function is that it is *invariant* under integer cycle changes (full revolutions), i.e.  $e^{i(\theta + 2\pi n)} = e^{i\theta}$ . Therefore, the initial integer ambiguities and (static data) cycle slips in the double difference carrier phase observations will have no influence on the value of the ambiguity function. The magnitude of the ambiguity function is then solely determined by the fraction of cycles. This is why the ambiguity function can be used for resolving the baseline vector and the ambiguities based on the ambiguous carrier phase data.

Apparently, if the trial position  $(x, y, z)$  equals the correct position  $(x_0, y_0, z_0)$  and if we further assume the observed and computed observations are error-free (which is not realistic but makes the illustration simple), the observed double difference observation  $\nabla\Delta\Phi^j(x_0, y_0, z_0)_{\text{obs}}$  of each satellite will exactly equal its corresponding computed double difference observation

$\nabla\Delta\Phi^j(x, y, z)_{\text{comp}}$  upon a difference of a constant integer of cycles that have no influence on the value of the ambiguity function or phasors. Under such a situation, the ambiguity function (5.1) will reach its maximum value of  $N-1$  (i.e.  $A(x_0, y_0, z_0) = N-1$ ) for a single epoch of observations with  $N$  observed satellites because in this case each phasor in (5.1) is identical, having the form  $e^{i0} = 1$ . For other trial positions  $(x, y, z) \neq (x_0, y_0, z_0)$ ,  $A(x, y, z) < N-1$ . If the observation errors or other kinds of errors are taken into account, the maximum value of the ambiguity function at  $(x_0, y_0, z_0)$  will be a little smaller than  $N-1$ , i.e.  $A(x_0, y_0, z_0) \approx N-1$ . Unfortunately, in the neighborhood around the correct position there may be some other trial positions at which the ambiguity function reaches a relative maxima. For example, a single phasor  $e^{i2\pi(\nabla\Delta\Phi^j(x_0, y_0, z_0)_{\text{obs}} - \nabla\Delta\Phi^j(x, y, z)_{\text{comp}})}$  may have the same value at the correct position  $(x_0, y_0, z_0)$  as it has at all other positions where the difference in the calculated distance between the  $j$ th satellite and the base satellite used in the double differencing changes by an integer number of wavelengths. To overcome this problem, the phase observations from different satellites, different epochs and even different carrier frequencies are combined together to compute the value of the ambiguity function at a certain trial position. When enough measurements from different satellites and epochs are combined, all the relative maximas will be suppressed except the one at the correct position  $(x_0, y_0, z_0)$ .

According to the above explanations, the ambiguity function method works as follows. Select a volume of space around the approximate estimate of the correct point. For example, the volume could be a cube with 2 metre sides or 1 metre sides depending on the accuracy of the approximate estimate of the position. The defined search cube must include the correct position or the technique will fail. This cube is then divided into a grid of points separated in all directions by 0.1 to 0.25 cycles of L1 frequency. At each trial point or grid point, the value of the ambiguity function is computed for all the measurements included in the computation. Note that each measurement could increment the value of the ambiguity function by at most unity. If at a trial point the contribution of one of the measurements is less than a

predetermined minimally acceptable value, e.g. 0.7, then this trial position cannot be the correct position and the next trial position is tested. The trial position at which the ambiguity function obtains the maximum value will almost certainly be the correct position if enough measurements are included in the computation. Mader (1990) has shown that for reliable instantaneous phase ambiguity resolution by using only one epoch of observations, simultaneous measurements from 7 to 8 satellites should be available in order to suppress all the false maximas of the ambiguity function. Once the correct position is obtained, the carrier phase ambiguities can then be calculated by using the corresponding measured carrier phase observations.

The determination of the search volume or the initial estimate of the correct position is important for the successful application of the ambiguity function method. Since the computation time impractically increases with the increase of the search volume, the initial estimate of the correct position should be as accurate as possible. In the static mode, the initial estimate of the position can be calculated by triple difference or double difference (floating ambiguity) least squares method based on the available phase observations. The obtained accuracy may be well below the 1 metre level for short baselines (Remondi, 1990). If the receiver is in motion, the approximate position at a kinematic epoch can be provided by the filter running with floating carrier phase ambiguities based on the updates of measured pseudo-ranges and carrier phase observations. A more accurate estimate (below 1.5 m at  $1\sigma$ ) is achievable when the phase-filtered pseudorange model or sequentially adjusted phase and pseudo-range model is used to compute the kinematic positions (Cannon, 1987).

## 5.2.2 Results of Phase Initialization by Ambiguity Function

Semi-kinematic data sets collected over a well-established traverse in the Kananaskis region near Calgary (e.g. Cannon et al, 1990) were used to test the ambiguity function method for carrier phase ambiguity initialization. The detailed description of the field tests are given in Chapter 6. The first field test was carried out on Day 222, 1990 and the second on Day 121, 1991.

In the data set of Day 121, 1991, there were 10 data gaps within the initial 8 minute static positioning session over the initial short baseline (32 metres). This was due to receiver malfunctioning at the master station. These data gaps caused discontinuities or cycle slips in the carrier phase observations of all the available satellites. Because there were too many cycle slips in the short observation span, the static batch least squares method was unable to resolve the correct initial double difference integer ambiguities. In this case, the ambiguity function method was chosen for the initial ambiguity determination since this method is not affected by cycle slips. Because only five satellites were visible and only L1 carrier frequency data was collected, 5 epochs of observations evenly distributed among the initial 8 minutes of static positioning data were used in the computation of the ambiguity function. The one metre cube around the initial position was searched with a grid step of 0.1 cycles of the L1 wavelength. This resulted in 125,000 trial positions to be tested. The computation time was surprisingly long. It took 1233 seconds or 21 minutes on a 386 micro-computer with 33 MHz clock speed and a 387 math-coprocessor. The resolved  $\nabla\Delta$  carrier phase ambiguities over the initial baseline are given in Table 5.1. When the search volume was decreased to a 0.5 metre cube, which brought 15625 trial positions to be tested, the corresponding computation time then dropped to only 154 seconds or 2.5 minutes.

SV No.	Resolved phase ambiguities (L1 cycles) ( Base sat. SV 11)
SV 02	738688.9269
SV 16	1001841.9916
SV 18	1108864.9352
SV 19	1064656.9996

Table 5.1 Resolved Initial Phase Ambiguities by the Ambiguity Function Method Using 5 Epochs of Observations from the Data Set on Day 121, 1991.

It can be seen that the estimated phase ambiguities in Table 5.1 are very close to integers. By rounding them to their nearest integers, we then attain the correct integer carrier phase ambiguities which are held fixed in the following kinematic GPS positioning unless they are affected by cycle slips.

The ambiguity function method can also be used for the carrier phase ambiguity initialization in the kinematic mode. For reliable instantaneous phase ambiguity resolution, simultaneous observations from 7 to 8 satellites at a single epoch should be available and included in the computation of the ambiguity function in order to suppress all the false maximum peaks of the function. Table 5.2 shows one example of phase ambiguity determination in kinematic mode. One epoch of L1 observations at 494792 seconds from the data set of Day 222, 1990 was used, where 7 satellites were available simultaneously with a GDOP value around 3. The vehicle was moving at a speed of 60 km/h. The distance between the roving and the master receivers was 1.7 km. The searching was carried out within a one metre cube around the approximate position of the roving receiver with a grid step 0.1 cycle (0.02 m ). This also brought 125,000 trial positions to be tested. However, when compared with the first example where five epochs of observations were combined, the computation time

was dramatically decreased in this single epoch search. It only took 154 seconds or 2.5 minutes on a 386 micro-computer with 33 MHz clock speed and a 387 math-coprocessor.

SV No.	Resolved phase ambiguities (L1 cycles) ( Base sat. SV 06)
SV 02	- 596929.9804
SV 12	411736.9784
SV 09	662742.9918
SV 11	- 541409.9890
SV 13	116458.9419
SV 18	- 398648.9204

Table 5.2 Resolved Phase Ambiguities by the Ambiguity Function Method in Kinematic Mode Using One Epoch of Observations on Day 222, 1990

The correct carrier phase integer ambiguities at this kinematic epoch were then obtained by rounding the estimated phase ambiguities in Table 5.2 to their nearest integers. Since no cycle slips occurred from the beginning to the present epoch (494792 seconds), the ambiguities obtained by the ambiguity function method were the same as the initial phase ambiguities resolved by the static batch least squares method at the beginning.

If less than 7 or 8 satellites are available simultaneously at a single epoch, multiple epochs of measurements from the moving receiver can be used together in the ambiguity function computation to suppress the false maximas. In this case, the change in observed phase between the epochs selected will be used to calculate the change in position of the moving receiver. These position changes will then be used for each position in the search volume at the first epoch to predict the position to be used for the ambiguity function

computation at the second and any subsequent epochs. Unlike the static case, no cycle slips are allowed between these kinematic epochs.

Table 5.3 shows one example where two epochs of measurements from kinematic mode were used in the computation of the ambiguity function to search the phase ambiguities. In the field test on Day 121, 1991, only five satellites were in view at the beginning of the session. This made the instantaneous phase ambiguity search by ambiguity function method unreliable due to the few measurements available at a single epoch. Therefore, observations from two epochs (330453 seconds and 330473 seconds) were combined in the computation of the ambiguity function. The distance between these two kinematic epochs was 251 metres. The search volume was a one metre cube with a grid of 0.02 m, which resulted in 125,000 trial positions. The computation time was 1326 seconds or 22 minutes. When the search volume was decreased to a 0.5 metre cube, the computation time was reduced dramatically to 165 seconds or 2.7 minutes.

SV No.	Resolved phase ambiguities (L1 cycles) ( Base sat. SV 11)
SV 02	738688.9997
SV 16	1001841.9943
SV 18	1108864.9872
SV 19	1064657.0003

Table 5.3 Resolved Phase Ambiguities by the Ambiguity Function Method in Kinematic Mode Using Two Epochs of Observations on Day 121, 1991

It can be seen that after rounding the ambiguities in Table 5.3 to their nearest integers, they are equal to the results given in Table 5.1. Since no cycle slips were found from the beginning of the kinematic mode to the present epochs, the carrier phase ambiguities should

remain unchanged. This is another proof that we have resolved the correct initial phase ambiguities in this surveying session.

From the above examples and test computations, we may conclude that the ambiguity function method is an accurate method for resolving carrier phase ambiguities, but the long computation time prohibits the use of this method in real-time applications. The computation time is mainly affected by two factors, the size of the search volume and the number of measurement epochs used in the function computation. In kinematic GPS surveys, it is difficult to obtain a search volume that is smaller than a one metre cube when cycle slips occur on all or most of the available satellites. If a large search volume has to be used at the beginning of the computations, we may first carry out the searching with a coarse grid (e.g.,  $0.25\lambda \sim 0.5\lambda$  spacing step) over the volume. Once a more accurate approximate position is obtained and thus a smaller search volume can be defined, a second search with a fine grid (e.g.,  $0.1\lambda$  spacing) can be conducted. Using this method, the computation time can be greatly reduced (Remondi, 1984). The number of measurement epochs used in the ambiguity function computations is another factor affecting the computation time. From a computational point of view, the single epoch case takes the least computing time, but 7 to 8 satellites in view simultaneously are needed for reliable phase ambiguity resolution. When the full 24 GPS satellites are in orbit by 1993, this requirement will be met at about 80% of the time each day. With the current available computing facilities, it seems that the ambiguity function method can only be used in the post kinematic GPS data processing stage.

## CHAPTER 6

### **TESTING AND RESULTS**

The computer program QUALIKIN has been developed by the author as part of this thesis. This program can perform the described reliability analysis, statistical testing and adaptation methods along with kinematic differential GPS position and velocity estimation. The implementation and structure of the program is first presented in this chapter. Its applicability for field data processing is then tested using the data collected over the traverse in Kananaskis Country with two Ashtech L-XII GPS receivers. The suitability as well as the limitations of the proposed testing and adaptation procedures for bias detection and correction in kinematic GPS surveying are also investigated in this chapter.

#### **6.1 DESCRIPTION OF THE PROGRAM QUALIKIN**

Based on the theories and algorithms given in the previous chapters, the post-mission program QUALIKIN for QUALity control analysis in KINematic GPS positioning has been developed. It runs on a micro-PC 386 computer and needs about 400K RAM. Most of the program was written in FORTRAN 77. The decoding and pre-processing segments were written in C-Langue. The whole program package consists of about 8000 code lines including the explanations and can be divided into two parts, the pre-processor and the main

processor. The function of the pre-processor is to decode the raw GPS binary data and create the standard input observation and ephemeris files required by the main processor. The main processor then processes the GPS data and outputs the desired quantities, such as the vehicle's position and velocity and the detected bias values. Generally speaking, the pre-processor is receiver-dependent. Different kinds of receivers need different pre-processors due to the different raw data structures coded in the receivers. The main processor, on the other hand, can process the data collected by different kinds of receivers as long as the pre-processor provides the observation and ephemeris data files with the required standard input formats of the main processor. Fig. 6.1 shows the flowchart of the main processor of the program QUALIKIN.

In addition to performing the reliability analysis, statistical testing and bias adaptation in kinematic GPS surveying, QUALIKIN can also process various kinds of differential GPS positioning data, such as static positioning data, semi-kinematic positioning data and kinematic positioning data. The batch least squares approach is utilized to process the static GPS data, while the Kalman filter given in Chapter 3, along with the statistical testing and adaptation procedures, is employed to process the kinematic GPS data. The mathematical correlations among the double difference observations are taken into account both in the batch least squares and in the Kalman filter measurement updates. The initial carrier phase ambiguities can be resolved in this program by any one of the following techniques: (1) surveying over a known baseline, (2) occupying an unknown initial baseline for 10-15 minutes to allow for a static solution, or (3) searching by the ambiguity function method.

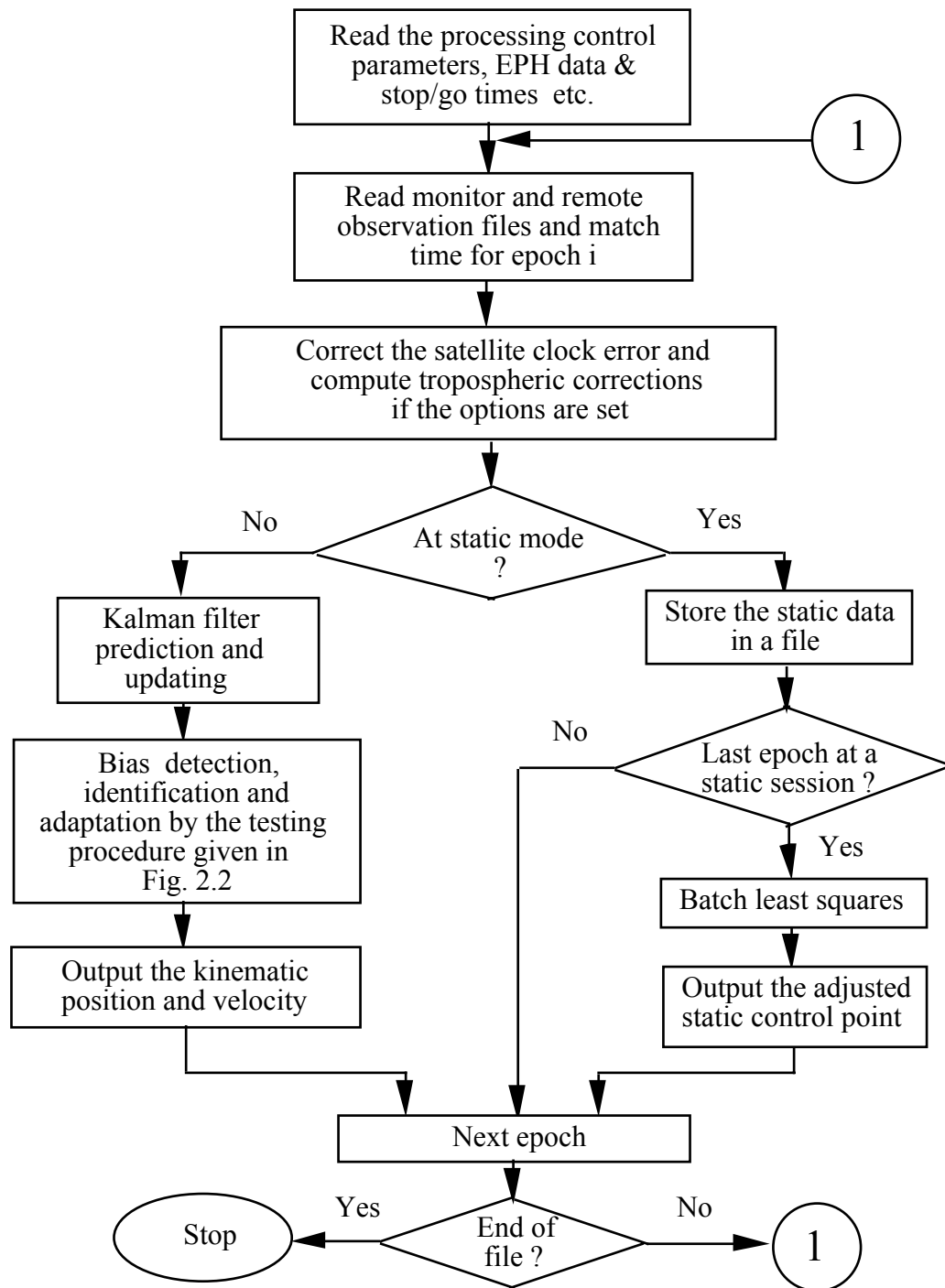


Fig. 6.1 Flowchart of the main processor of the program QUALIKIN

In the statistical testing and bias estimation and adaptation modules, only the statistics for testing observation biases, such as cycle slips in carrier phase, outliers in pseudorange and outliers in the phase rate measurement, are implemented in this program system because for most of the kinematic GPS surveying tasks, the constant velocity or constant acceleration model seems adequate with high data rate ( $\geq 1$  Hz) GPS receivers now available. The testing procedures coded in these modules are already given in Fig. 2.2 of Chapter 2. If biases in the GPS observations are detected and identified, the bias estimation and adaptation steps are then carried out. If a loss of lock on all satellites occurs or cycle slips are found on most of the available satellites and the filter itself cannot resolve the correct phase ambiguities, an ambiguity search by ambiguity function method (AFM) is then invoked within the program.

A final remark should be made about the detection and estimation of carrier phase cycle slips in kinematic GPS observations. Generally speaking, a cycle slip may occur under two situations: (i) a cycle slip between two consecutive epochs, which does not result in a lost measurement to that satellite (i.e. relock again before the second epoch); and (ii) a cycle slip between measurement gaps, which means that we lose track (no measurements) on a satellite for several epochs and resume track again afterwards. For the first situation, we have to first detect and then estimate the cycle slips. But for the second situation, the detection step is not necessary because we are almost sure that a gap in the collected data set suggests a cycle slip has occurred on the corresponding satellite. In this case, only the estimation step for cycle slips (or new phase ambiguity) is needed upon relocking on the satellite. Once the cycle slip or the new ambiguity is estimated and resolved, its correctness, or its internal consistency with other observations, is tested by the given statistics in the following epochs.

## **6.2 DESCRIPTION OF THE FIELD TESTS**

The University of Calgary traverse located along Highway 40 in the Kananaskis region was used to test the testing procedures and the program. Eight control points, about 1 km apart within this traverse, had been previously established with a relative accuracy 2-5 cm using static differential GPS techniques (Cannon et al, 1990). Offset points from the known traverse points were also established on both sides of the Highway to provide easy access for a vehicle. The sketch of the offset points is shown in Fig. 6.2. These known control points were utilized for comparison with the positioning results obtained by the program QUALIKIN.

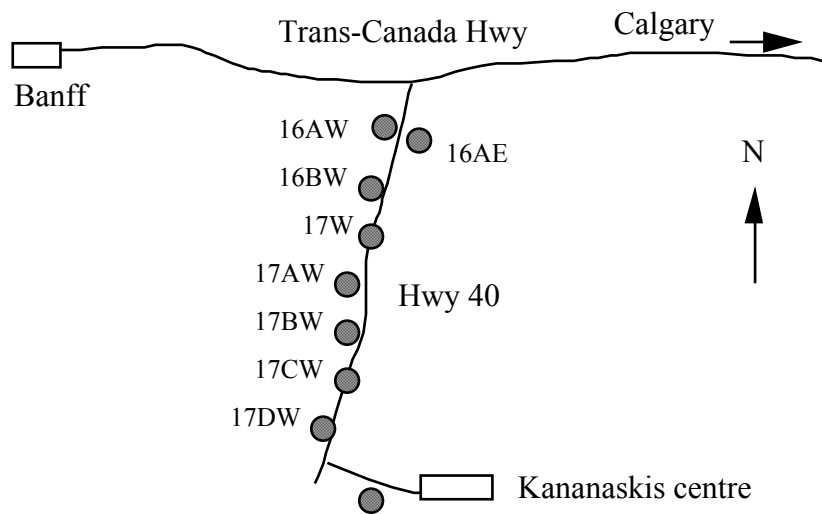


Fig. 6.2 Sketch of the Test Traverse Control Points

Field tests were carried out on Day 222, summer 1990 and Day 121, spring 1991 in differential *semi-kinematic* (stop/go) surveying mode. Two Ashtech LD-XII receivers, owned by the Department of Surveying Engineering, were used to collect data. These up-to-date receivers have 12 tracking channels and a maximum of 2 Hz data rate. Therefore, all-in-view GPS satellites could be tracked simultaneously. During the tests, the initial baseline, which is about 30 m long from point 16AW (as master station) to 16AE, was first occupied for about 10 minutes to allow for the baseline vector and carrier phase ambiguity resolution. The antenna

of the moving receiver was then hand carried from the starting control point, mounted on the car roof and driven to the next control point. On arrival at the next control point, the antenna was moved from the car roof onto the control point performing 2-3 minute static positioning. This procedure was repeated until all the control points were visited. When the vehicle travelled from one point to another point, the receiver kept on tracking the satellites and collecting the data so that the vehicle's position and velocity in kinematic mode could be determined. In both tests, the maximum vehicle speed reached about 80 km h<sup>-1</sup>. On Day 222, 1990, L1 data were collected at a 4 second interval, while on Day 121, 1991, the data logging interval was changed to 1 second. The detailed observation information of these field tests is given in Table 6.1.

Day	Data Rate	Satellites Observed	Duration of Test	Dilution of Precision	
				HDOP	VDOP
222 (1990)	4 sec.	SVs 2, 6, 9, 11, 12, 13, 18	62 min.	1.35~1.01	2.46~1.60
121 (1991)	1 sec.	SVs 2, 6, 11, 16, 18, 19	48 min.	1.42~1.45	2.25~2.87

Table 6.1 Observation Information for the Semi-Kinematic Tests

### 6.3 POSITIONING RESULTS

The differential GPS data sets collected in the field tests were processed using the developed program system QUALIKIN with the statistical testing functions performed. The differences between the obtained coordinates of the control points and the known ground truth provide a first check and evaluation of the proposed processing techniques and the written program. The independent assessment of the kinematic positioning results between the control points is however impossible in this case, since no other kinematic positioning systems with

compatible accuracy could be used during the tests. But in order to provide some kind of check and comparison for the kinematic positioning results obtained by QUALIKIN with the statistical testing method performed, the same data sets were processed using the program KINSRVY which comes with the Ashtech GPPS suite of programs. The outputs of the kinematic positioning results from both QUALIKIN and KINSRVY were compared to give an internal performance evaluation of the developed program and the testing algorithms as done previously between SEMIKIN and KINSRVY (Cannon et al , 1990).

### **6.3.1 Day 222 Results**

The data set collected on Day 222, 1990 was considered very good. The average HDOP and VDOP values were about 1.35 and 2.5, respectively. Up to 7 satellites were in view most of the time during the session. The double difference initial phase ambiguities were correctly resolved by batch least squares method using the 10 minute static data over the initial baseline which was held unfixed. SV 06 was chosen as the base satellite for double differencing. The constant acceleration model was adopted as the system model in the kinematic data processing with the spectral densities  $0.05 \text{ m}^2 \text{ s}^{-5}$  for all three acceleration states ( $\delta a_n$ ,  $\delta a_e$ ,  $\delta a_h$ ). Fig. 6.3 shows the agreement at the control points.

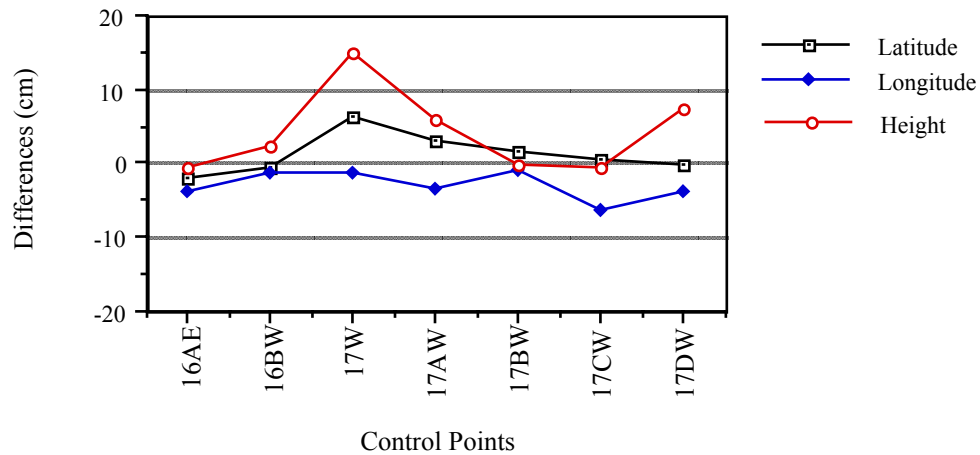
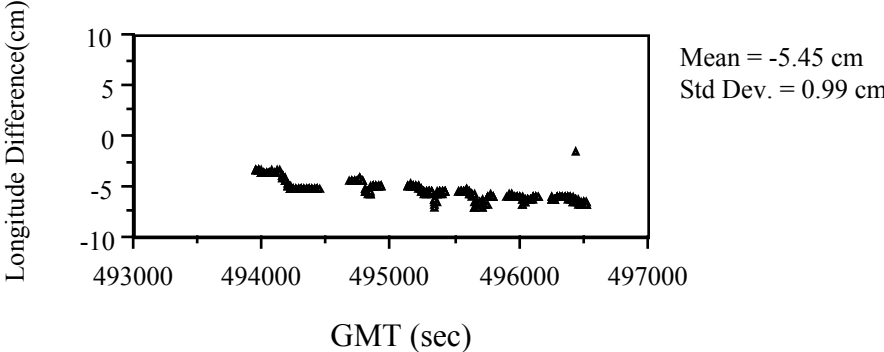
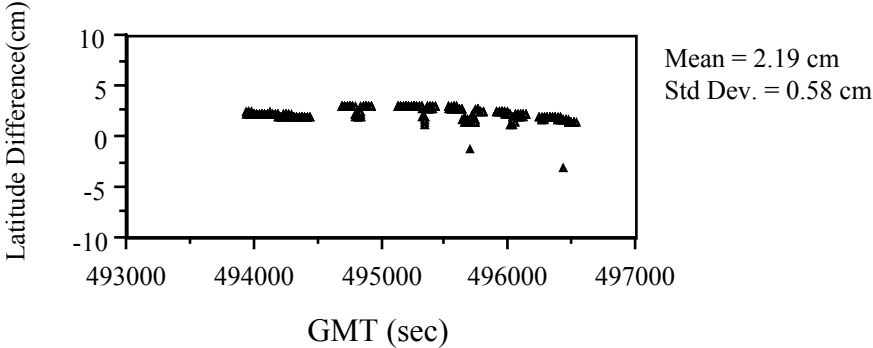


Fig. 6.3 Position Differences with the Control Points for Day 222

Differences with the known control points were generally less than 5 cm except in height on two points, 17W and 17DW. The root mean squares (rms) computed using the differences with the known control points were 2.82 cm in latitude, 3.44 cm in longitude and 6.73 cm in height.

The accuracy of kinematic position and velocity estimation could not be checked independently due to the lack of extra positioning systems in this project. The internal accuracy output from the Kalman filter were good. The standard deviations were about 1.5 cm in latitude, 1.2 cm in longitude and 3.6 cm in height. For velocity estimation, the standard deviations were about  $5 \text{ cm s}^{-1}$  in northing,  $4 \text{ cm s}^{-1}$  in easting and  $11 \text{ cm s}^{-1}$  in up direction. The comparison of the kinematic positions obtained by QUALIKIN and KINSRVY at each epoch is plotted in Fig. 6.4. The agreement of the results is within 7 cm in all three dimensions, which is the same level as between KINSRVY and SEMIKIN (Cannon et al, 1990).

For statistical testing, only two outliers in pseudorange observations were detected and estimated. One outlier was 23.60 m on SV 02 at 493976 seconds. The other was 25.34 m on SV 12 at 495796 seconds. Since the MDB value for pseudoranges was about 18 metres in this surveying session, only the outliers or multipath effects that were larger than 18 metres on pseudoranges could be detected as biases. In this data set, SV 02 and SV 12 did have numerous phase losses (data gaps) due to the lower satellite elevation and forest shadow. But their new phase ambiguities upon relock of the satellites were resolved correctly in the program using the redundant satellites. No other cycle slips in the carrier phases were found.



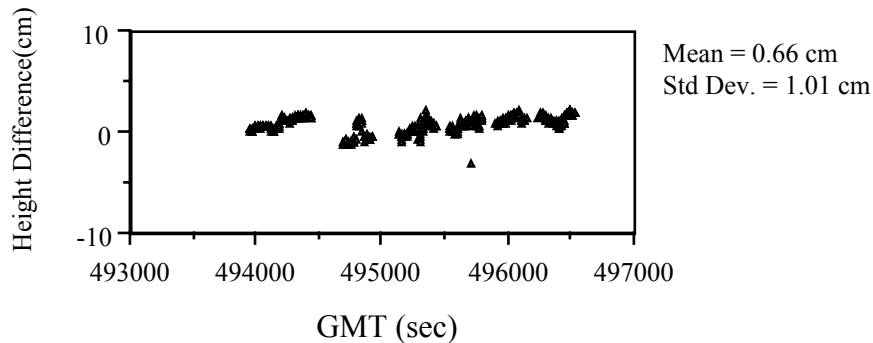


Fig. 6.4 Differences Between QUALIKIN and Ashtech KINSRVY for Kinematic Results of Day 222, 1990

### 6.3.2 Day 121 Results

There were 12 occasions in the data set collected on day 121, 1991 that all satellites simultaneously lost phase lock for 5 to 15 seconds due to receiver malfunctioning at the master station. This made the data processing very difficult. As described in Chapter 5, the initial carrier phase ambiguities were resolved by ambiguity function method (AFM), since there were 10 data gaps within the initial 8 minutes of static positioning. During the following kinematic and semi-kinematic data processing, the ambiguity re-initialization by AFM was performed twice at control points 16BW and 17CW due to the occurrences of phase losses on all the satellites. Since the data rate was 1 second, the constant velocity model was used as the system model in the kinematic data processing with the spectral densities  $0.2 \text{ m}^2 \text{ s}^{-3}$ ,  $0.2 \text{ m}^2 \text{ s}^{-3}$  and  $0.1 \text{ m}^2 \text{ s}^{-3}$  for three velocity states  $\delta V_n$ ,  $\delta V_e$  and  $\delta V_h$  respectively. Fig. 6.5 shows the agreement at the control points.

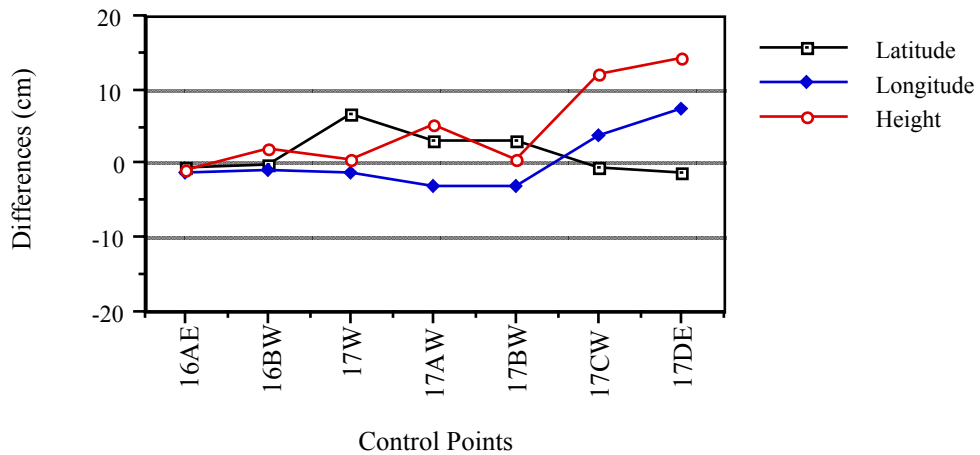


Fig. 6.5 Position Differences with the Control Points for Day 121

It can be seen that the differences with the known control points are generally within 5 cm except in the height component. The rms are 3.1 cm in latitude, 3.6 cm in longitude and 7.4 cm in height. The results from these two field tests provided a good check of the positioning repeatability of the suggested processing method and the GPS system.

In this data set, one outlier in pseudorange observations was found at 332227 seconds on SV 18 with the bias value 21.3 metres. No other cycle slips were found other than the data gaps in the carrier phase observations. The internal accuracy of the kinematic positions was about 1.5 cm, 1.2 cm and 3.5 cm for latitude, longitude and height respectively. The comparison of the kinematic positioning results with the output of KINSRVY was not given here due to the frequent restarts in the KINSRVY execution caused by the frequent carrier phase losses.

#### 6.4 DETECTION AND ADAPTATION FOR SIMULATED BIASES

In this section, different observation biases, such as cycle slips in carrier phases between consecutive epochs, outliers in pseudoranges, and outliers in phase rates, are deliberately introduced in the real data sets collected in the field experiments in order to evaluate the bias detection ability of the proposed statistical testing procedures coded in the program system QUALIKIN. Cycle slips in carrier phases, which is one of the limiting factors in high precision kinematic GPS positioning, sometimes can be easily detected. For instance, in the data gap situation or loss-relock on a satellite case, a simple data editing method like phase prediction, which is to compare the predicted carrier phase with the measured one (Cannon, 1987), would be able to detect the cycle slip because in this case the cycle slip may amount to hundreds or even thousands of cycles. In real data processing, we always detect and correct the *large* part of a cycle slip by some simple data editing methods. The purpose of statistical testing is then to detect and correct the remaining *small* part of the cycle slip or the other small cycle slips in the observations. Once the cycle slip or the new ambiguity on a satellite is estimated and applied on the following carrier phase observations, its correctness or its internal consistency with the observations of other satellites is checked by monitoring the filter performance using the testing statistics. This is the reason why statistical testing is considered to be a quality control method in kinematic GPS positioning.

#### **6.4.1 Detection and Adaptation for Simulated Cycle Slips**

In the following computations, cycle slips on a *single* satellite and on *multiple* satellites were simulated at the *kinematic* epochs between the control points 16AE and 16BW, where the vehicle was accelerating. The simulated cycle slips on the corresponding satellites were at the one cycle level (19.02 cm).

Table 6.2 summarizes the detection and estimation results for simulated cycle slips in the data set of Day 121, 1991. The MDB analysis shows that the minimum detectable cycle slips in a single satellite case is about 0.5 cycle. Therefore, one cycle slip was added to the carrier phase observations on the corresponding satellites starting at the epoch time 330456 (GMT seconds), where the vehicle was moving at a speed of 36 km h<sup>-1</sup> and with an acceleration of about 1 m s<sup>-2</sup>. Five satellites (SVs 02, 11, 16, 18, 19) were simultaneously tracked and the data rate was 1 second. SV 11 was used as the base satellite in double differencing. The system model adopted in processing was the constant velocity model.

Case	Satellites with cycle slips		Detect	Identify	Final estimated bias values(Cycles)		
	No. of satellites	SV No.			SV No.	Estimated value	True value
1	Single sat.	SV 02	yes	yes	SV 02	- 0.964	- 1.00
2	Two sat.	SV 02 SV 18	yes	yes	SV 02 SV 18	- 1.265 + 0.801	- 1.00 +1.00
3	Three sat.	SV 02 SV 18 SV 16	yes	yes	SV 02 SV 18 SV 16	- 1.078 0.883 0.785	- 1.00 +1.00 +1.00
4	All sat.	SV 02 SV 18 SV 16 SV 19	yes	yes	SV 02 SV 18 SV 16 SV 19	- 1.115 0.748 0.865 1.055	- 1.00 +1.00 +1.00 +1.00

Table 6.2 Results of Cycle Slip Detection and Estimation for Simulated Cycle Slips in the Data Set of Day 121, 1991 (1 Second Data Rate).

From Table 6.2, we can see that in all cases the one cycle level slips in carrier phase observations could be correctly detected, identified and estimated. After rounding the estimated cycle slips to their nearest integer, we arrived at the exact simulated cycle slip values in the data set. These results indicate that the proposed statistical testing procedure is effective in carrier phase cycle slip detection and identification with data sets of one second data rate or higher, when a constant velocity model is used. In this case, the acceleration disturbance in the system model, i.e. constant velocity model, can be allowed to reach  $1\sim 2 \text{ m s}^{-2}$ , which are the usual accelerations in the land vehicle case.

Unfortunately, the above conclusions do not always hold for data sets with slower data rate intervals (e.g. 4 second data rate), especially when the vehicle is accelerating. This is due to the influences of system biases that are not modelled in the constant velocity model or constant acceleration model. The longer the data rate interval, the poorer the applicability of these system models.

Table 6.3 shows the results of cycle slip detection and estimation for simulated cycle slips in the Day 222, 1990 data set. Six satellites were observed at a 4 second data rate. The system model was the constant *acceleration* model. One cycle level slips were added to the carrier phase observations of the corresponding satellites starting at the time 494144 seconds, when the vehicle was moving with an acceleration of about  $0.33 \text{ m s}^{-2}$ .

From Table 6.3 and other testing runs, we observe that under small accelerations, usually less than  $0.3 \text{ m s}^{-2}$ , the statistical testing procedure can correctly detect, identify and estimate the one cycle level slip occurring on a *single* satellite in a data set with a 4 second data rate. When the number of satellites with simultaneous cycle slips increases to four or the number of satellites without slips decreases to 3, the statistical testing procedure can detect that there are some problems in the data set, but sometimes cannot identify the satellites which have one cycle level slips, as shown in Case 4 and Case 5 of Table 6.3. This is caused by the

influences of the unmodelled system biases, and also by the corresponding increase of the MDB values on each satellite as the number of biases increases. With more satellites having cycle slips and with longer measurement update intervals, the system bias effects and the observation bias effects are interwoven in a complicated manner. This makes the identification or isolation of small cycle slips on different satellites a very difficult task in kinematic data processing.

Case	Satellites with cycle slips		Detect	Identify	Final estimated bias values(Cycles)		
	Num. of satellites	SV No.			SV No.	Estimated value	True value
1	Single sat.	SV 02	yes	yes	SV 02	1.001	+1.00
2	Two sat.	SV 02 SV 18	yes	yes	SV 02 SV 18	1.012 0.968	+1.00 +1.00
3	Three sat.	SV 02 SV 18 SV 13	yes	yes	SV 02 SV 18 SV 13	1.012 1.040 - 0.940	+1.00 +1.00 - 1.00
4	Four sat.	SV 02 SV 18 SV 13 SV 09	yes	no (only 3 sat. 2,9,13 signified with cycle slips)	(Correctly identified when cycle slips increase to 5 cycle level )		+1.00 +1.00 - 1.00 - 1.00
5	All sat.	SV 02 SV 18 SV 13 SV 09 SV 11	yes	no (only 3 sat. 2,9,13 signified with cycle slips)	(Correctly identified when cycle slips increase to 5 cycle level )		+1.00 +1.00 - 1.00 - 1.00 +1.00

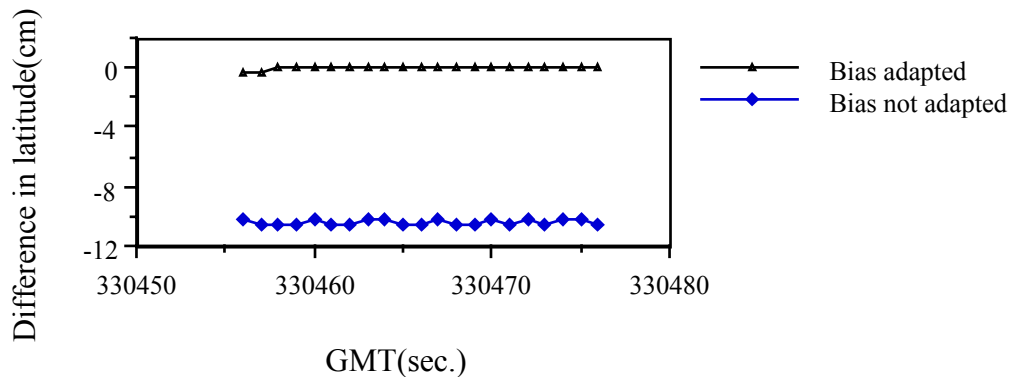
Table 6.3 Results of Cycle Slip Detection and Estimation for Simulated Cycle Slips in the Data Set of Day 222, 1990 (4 Second Data Rate).

The situation is much improved when the cycle slips on each corresponding satellite is increased to the 5 cycle level. In this case, all cycle slips in Case 4 and Case 5 defined in Table 6.3 can be correctly detected and identified. But the estimated cycle slips on some satellites, when rounded to their nearest integer values, may differ within the one cycle level from their true values. In some extreme situations, when the acceleration changes between epochs

exceeds  $1 \text{ m s}^{-2}$ , we may even fail to correctly identify the one cycle level slip on a single satellite case in the data set with 4 second data rate. Therefore, the high data rate (e.g. 1 second or higher) is required for cycle slip detection and identification at the one-cycle level in a highly dynamic environment.

Once the biases are detected, identified and estimated at a certain epoch, the adaptation or correction of the bias influences on the corresponding Kalman filtering results can be immediately carried out by the given two-stage Kalman filter algorithm.

Figure 6.6 shows part of the results of cycle slip adaptation for the single satellite case, i.e. Case 1 given in Table 6.2. In this figure, the cycle slip free positioning results were used as a reference. The differences between the results *with* and *without* cycle slips adaptation by the two-stage Kalman filter method are plotted separately in order to show the effectiveness of the adaptation procedure. Only 21 epochs of kinematic results are plotted in this figure.



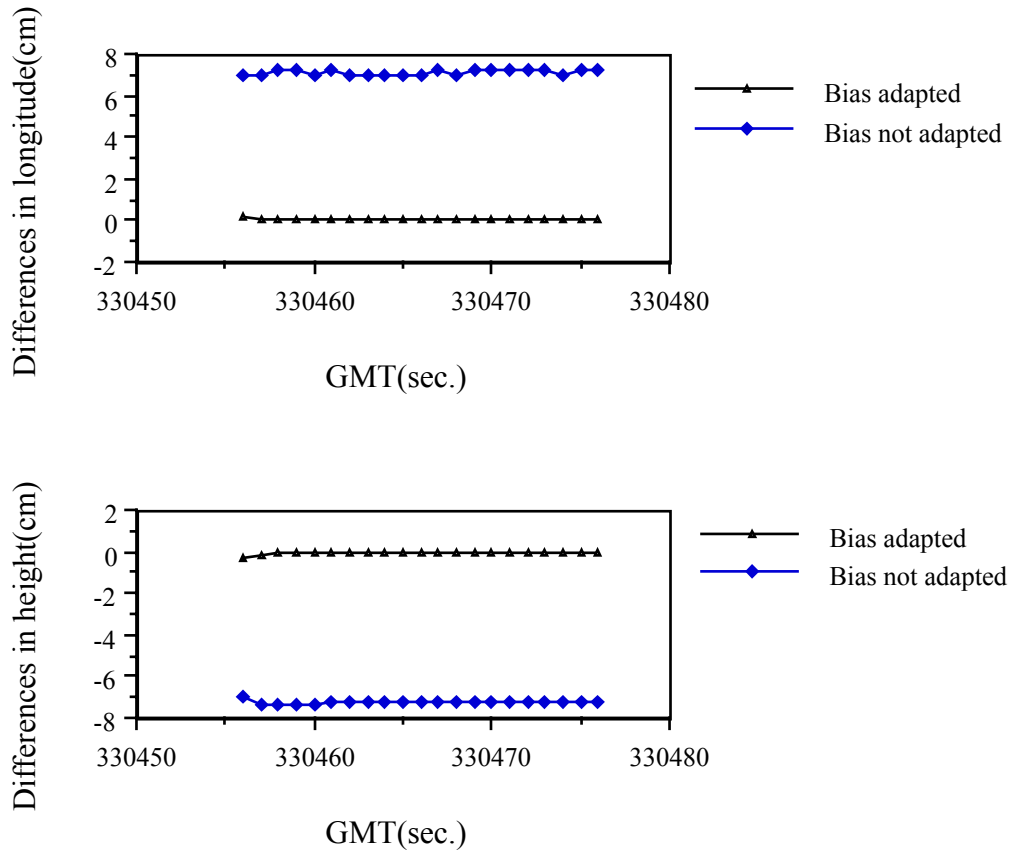


Fig. 6.6 Comparison of the Results with and without Cycle Slip Adaptation for the Single Cycle Slip Case

Fig. 6.6 clearly shows that the bias adaptation method eliminates the cycle slip influences on the positioning results output by the Kalman filter. Also, from the results without detection and adaptation for the simulated bias, it can be seen that the position errors caused by the cycle slips change very little from epoch to epoch within this short (21 seconds) observation span. This is due to the little change and nearly constant satellite geometry within this short time. The magnitudes of the influence at the first epoch with the cycle slips present were -10.2 cm, 7.0 cm and -7.3 cm for latitude, longitude and height respectively. These magnitudes of the cycle slip influences well match the theoretical influence values of -10.4 cm,

7.1 cm and -7.2 cm in latitude, longitude and height respectively, which are computed by the influence analysis formulas given in Chapter 2. The cycle slips influences on the velocity states are practically zero and thus not plotted.

#### **6.4.2 Detection and Adaptation for Simulated Outliers in Phase Rate Observations**

Outliers in phase rate observations mainly affect the velocity determination in kinematic GPS surveys. In order to access the ability of the testing procedure to detect the phase rate outliers, different situations were simulated with the data set of Day 121, 1991. In this data set, the worst minimum detectable outlier (MDB) on a single satellite was about  $0.5 \text{ m s}^{-1}$ . Therefore, the phase rate outliers at the level of  $0.95 \text{ m s}^{-1}$  were simulated on a single satellite as well as on multiple satellites at the epoch time 330456, where the vehicle travelled with an acceleration of about  $1 \text{ m s}^{-2}$ . Table 6.4 shows the results of the phase rate outlier detection, identification and estimation. The system model used is the constant velocity model.

Case	Satellites with phase rate outliers		Detect	Identify	Final estimated bias values (m/s)		
	Num. of satellites	SV No.			SV No.	Estimated value	True value
1	Single sat.	SV 02	yes	yes	SV 02	- 0.957	- 0.95
2	Two sat.	SV 02 SV 18	yes	yes	SV 02 SV 18	- 1.080 + 0.858	- 0.95 +0.95
3	Three sat.	SV 02 SV 18 SV 16	yes	yes	SV 02 SV 18 SV 16	- 1.036 0.857 1.023	- 0.95 +0.95 +0.95
4	All sat.	SV 02 SV 18 SV 16 SV 19	yes	yes	SV 02 SV 18 SV 16 SV 19	- 0.886 0.915 1.234 1.082	- 0.95 +0.95 +0.95 +0.95

Table 6.4 Results of Bias Detection and Estimation for Simulated Phase Rate Outliers in the Data Set of Day 121, 1991 (1 Second Data Rate).

Table 6.4 shows that in all cases the outliers in phase rate observations can be correctly detected and identified. The estimated outliers are very close to the true values. Therefore, the phase rate outlier influences on the velocity determination can be well eliminated by the testing and adaptation procedure in a data set with a high data rate.

### 6.4.3 Detection and Adaptation for Simulated Outliers in Pseudorange Observations

Pseudorange outliers are likely to occur in a multipath environment. They mainly affect the position determination in GPS kinematic surveys. Fortunately, their influence on the

estimated positions are practically negligible in the combined processing of carrier phase and pseudorange observations. This is due to the much lower observation precision of pseudoranges as compared to carrier phases. Table 6.5 gives the results of detection and estimation for the simulated pseudorange outliers in the data set of Day 121, 1990. The MDB value for individual pseudorange outliers in this data set is about 18 m when using a standard deviation of 4 metres for single difference pseudorange observables. Therefore, 30 m outliers were added on the corresponding observations at epoch time 330456 seconds.

Table 6.5 and the other simulated runs show that the testing procedure can correctly detect and identify the single pseudorange outlier case if the pseudorange bias is greater than its corresponding MDB value. However, as the number of satellites with outliers increases, the detectability for multiple outliers becomes poorer. This is because the rapid increase of the MDB values in a multiple outlier situation due to the much lower observation precision of pseudoranges. In Case 4 of Table 6.5, only if the outliers on all the satellites increase to 80 m, can the testing procedure correctly detect, identify and estimate all the simulated biases. However, even with the 80 m pseudorange outliers on all the satellites left uncorrected, the influence on the estimated kinematic position is only about 0.136 cm.

Case	Satellites with pseudorange outliers		Detect	Identify	Final estimated bias values (m)		
		SV No.			SV No.	Estimated value	True value
1	Single sat.	SV 16	yes	yes	SV 16	24.903	30.00
2	Two sat.	SV 16 SV 18	yes	yes	SV 16 SV 18	24.933 30.120	30.00 30.00
3	Three sat.	SV 02 SV 18 SV 16	yes	no (Only two sat. identified 2,18)			30.00 30.00 30.00
4	All sat.	SV 02 SV 18 SV 16 SV 19	no	no	(Correctly detect and identify when biases increase to 80 m )		30.00 30.00 30.00 30.00

Table 6.5 Results of Bias Detection and Estimation for Simulated Pseudorange Outliers in the Data Set of Day 121, 1991 (1 Second Data Rate).

## CHAPTER 7

### CONCLUSIONS AND RECOMMENDATIONS

In precise kinematic GPS surveys, a quality control method is inevitably needed for real-time data processing because of the possibility of biases like carrier phase cycle slips and outliers in phase rate and pseudorange measurements. In this thesis, the statistical quality control method for use in kinematic GPS positioning based on the state space models was investigated. Firstly, the general recursive formulas for bias influence analysis and reliability analysis (MDB) were derived for the Kalman filter design. Then a real-time statistical testing and adaptation procedure was developed based on the two-stage Kalman filtering technique, hypothesis testing theory and reliability analysis concept. This procedure introduced a new step of bias confirmation by using the concept of minimum detectable bias (MDB) and aimed to automatically detect the common observation biases and eliminate their influences on GPS kinematic positioning results. All the derived formulas and algorithms were implemented in a software package QUALIKIN and tested using real GPS data sets collected in the field tests.

The bias influence analyses show that carrier phase cycle slips affect mainly the estimated positions, while the phase rate outliers affect mainly the estimated velocities. Cycle slips in double difference observables have a severe long-term influence on position estimation. Therefore, real-time correction and adaptation for this kind of bias is necessary to assure the correctness of the kinematic positioning results. Instantaneous outliers in the

observation and system models, on the other hand, only affect the current and the following few epochs of the filtering results. This means that the Kalman filter can reduce automatically the effects of instantaneous outliers after a few epochs of measurement updates. In the combined processing of carrier phase, pseudorange and phase rate observations, the influence of outliers in C/A code pseudoranges on GPS positioning results is negligible due to the much lower measurement precision of pseudoranges. However, the proposed testing procedure can still detect pseudorange outliers of the order of 18 m present on a *single* satellite (assuming 4 m observation precision assigned to single difference pseudoranges ). This provides some control on large multipath effects along a surveying trajectory.

The minimum detectable bias (MDB) analysis of kinematic GPS surveys indicates that the observation biases detectable by statistical testing is basically a function of the satellite geometry and the measurement precision. The MDB shows the minimum bias value that the statistical testing method can detect with a predetermined probability for an individual bias, under the assumption that no other bias except the concerned one is present in the system and observation models. In this sense, the MDB analysis together with the bias influence formulas in the Kalman filtering provides a useful tool for kinematic and dynamic system design.

The implementation and testing of the developed statistical quality control method in kinematic GPS positioning software was an essential part of this research. The program package QUALIKIN developed by the author can perform the reliability (MDB) analysis and real-time statistical testing and bias adaptation in kinematic differential GPS surveying. It can also process static and semi-kinematic differential GPS data. The successful processing of the real semi-kinematic data sets collected from two field tests shows the suitability and the applicability of the developed program system and the derived testing procedure.

The investigation of the detection of simulated biases between consecutive epochs indicates that, with a data rate of one second or higher, the testing procedure can correctly

detect, identify and estimate cycle slips occurring at the one cycle level on multiple satellites under normal land vehicle motion scenarios. Also, under the same assumption, the testing procedure can effectively detect outliers at the  $1 \text{ m s}^{-1}$  level in phase rate observations on multiple satellites and eliminate their effects on the filtering results. However, the above conclusions are not always true for data sets with slower data rate intervals (e.g. 0.25 Hz), especially when the vehicle is accelerating. This is due to the influence of the system biases that are unmodelled in the constant velocity model or constant acceleration model. The longer the data rate interval, the poorer the applicability of these system models. Therefore, a high data output rate, e.g. 1 second or higher, is recommended for the detection and identification of small cycle slips in a high dynamic environment of land vehicle motion.

Since it is the first time that statistical quality control methods have been used and tested in the kinematic GPS data processing, there are a number of problems left to be studied further. The first would be the incorporation of detection and adaptation of system model biases in the proposed testing procedure for high dynamic surveying and navigation environments. Based on the theoretical formulas developed herein, it is easy to do this in the testing procedure but it requires an elaborate and complicated bias search algorithm to distinguish between the observation bias and system bias. The extension of the statistical testing method to the smoothing algorithm would be useful for kinematic GPS data post-processing and thus needs investigation. The other problem of interest would be the application of the quality control methods to some other integrated systems such as GPS/INS. In this kind of systems, the system model could be more accurately described than that of a sole GPS positioning system and we would have more redundant measurements available. Thus, the results of statistical testing would be more accurate and reliable. The third problem to be investigated further is the carrier phase ambiguity resolution in kinematic mode, i.e. "on the fly" ambiguity resolution. In cases where long data gaps are present on all available satellites in kinematic mode, no methods up to now can satisfactorily resolve the new phase

ambiguities by using GPS alone. Some promising and efficient techniques to handle this problem are to use precise integrated systems (Cannon, 1991 ) or to use the P-code GPS receivers. More tests with the high data rates (e.g., 2 ~ 4 Hz) are needed in order to fully evaluate the ability of the statistical quality control methods. With the improvement of GPS technology, the enhancement of the processing methods and the full deployment of the GPS constellation in the near future, kinematic GPS positioning is expected to achieve reliable and accurate results and find wider applications.

## REFERENCES

- Baarda, W. (1968): "A Testing Procedure for Use in Geodetic Networks." Netherlands Geodetic Commission, Publications on Geodesy, New Series 2, No. 5 Delft.
- Basseville, M. (1988): "Detecting Changes in Signals and Systems -- A Survey." *Automatica* ,Vol. 24, No. 3, pp.309-326
- Cannon, M.E. (1987): "Kinematic Positioning Using GPS Pseudo-range and Carrier Phase Observations." UCSE Report No. 20019, The University of Calgary.
- Cannon, M.E. (1990): "High Accuracy GPS Semi-kinematic Positioning: Modelling and Results." *Navigation* , Journal of the Institute of Navigation, Vol. 37, No. 1.
- Cannon, M.E. (1991): "Airbone GPS/INS with an Application to Aerotriangulation." UCSE Report No. 20040, The University of Calgary.
- Cannon, M.E., G., Lachapelle, H., Eyers and K.P., Schwarz (1990): " A Comparison of SEMIKIN and KINSRVY for Kinematic Applications." Proc. of ION GPS-90, Colorado Springs, Colorado.
- Casparly, W.F. (1987): "Concepts of Network and Deformation Analysis." Monograph 11, School of Surveying, UNSW, Australia.

- Counselman, C.C. and S.A. Gourevitch (1981): "Miniature Interferometer Terminals for Earth Surveying: Ambiguity and Multipath with Global Positioning System." *IEEE Transactions on Geoscience and Remote Sensing*, Vol. GE-19, No. 4.
- Frank, P. (1990): "Fault Diagnosis in Dynamic Systems Using Analytical and Knowledge-based Redundancy--A Survey and Some New Results." *Automatica* Vol. 26, pp. 459-474.
- Friedland, B. (1969): "Treatment of bias in recursive filtering." *IEEE Trans. Automat. Contr.* Vol. AC-14, Aug. 1969.
- Gelb, A. (Ed.) (1974): *Applied Optimal Estimation*. The M.I.T. Press, Cambridge, Mass.
- Hatch, R. (1990): "Instantaneous Ambiguity Resolution." Proceedings of IAG International Symposium 107 on Kinematic Systems in Geodesy, Surveying and Remote Sensing, Springer Verlag, New York.
- Hofmann-Wellenhof, B. and B.W. Remondi (1988): "The Antenna Exchange: One Aspect of High-Precision GPS Kinematic Survey." Presented at International GPS Workshop, Technische Hochschule, Darmstadt, FRG, April 10-13, 1988.
- Hwang, P.Y.C. and Brown, R.G. (1990): "GPS Navigation: Combining Pseudo-range with Continuous Carrier Phase Using a Kalman Filter." *Navigation*, Vol. 37, No. 2.
- Ignagni, M.B. (1981): "An Alternative Derivation and Extension of Friedland's Two-stage Kalman Estimator." *IEEE Trans. Automat. Contr.* Vol. AC-26, No.3.
- Krakiwsky, E.J. (1990) : "The Method of Least Squares: A Synthesis of Advances." Lecture Notes, Dept. of Surveying Engineering, The University of Calgary, Calgary, Canada.
- Lachapelle, G., W., Falkenberg, D., Denfeldt, P., Kielland (1989): "Marine DGPS Using Code and Carrier in a Multipath Environment." Proceedings of the satellite division of ION GPS'89, Colorado Springs, Colorado.
- Lachapelle, G. (1990): "GPS Observables and Error Sources for Kinematic Positioning." Proceedings of IAG International Symposium 107 on Kinematic Systems in Geodesy, Surveying and Remote Sensing, Springer Verlag, New York.

- Li, D. (1986): "Trennbarkeit und Zuverlässigkeit bei zwei verschiedenen Alternativhypothesen im Gauss-Markoff Modell." *ZfV*, Heft 3, Vol. 111, pp114-127.
- Lu, G. and G., Lachapelle (1990): "Reliability Analysis for Kinematic GPS Position and Velocity Estimation." Proceedings of IAG International Symposium 107 on Kinematic Systems in Geodesy, Surveying and Remote Sensing, Springer Verlag, New York.
- Mader, G. (1990): "Ambiguity Function Techniques for GPS Phase Initialization and Kinematic Solutions." Proceedings of the Second International Symposium on Precise Positioning with the Global Positioning System, Ottawa, Canada, Sept. 1990.
- Mehra, R.K. and J., Peschon (1971): "An Innovations Approach to Fault Detection and Diagnosis in Dynamic Systems." *Automatica*, Vol. 7, pp. 637-640.
- Pelzer, H. (Herausg.) (1985): *Geodätische Netze in Landes- und Ingenieurvermessung II*. Wittwer Verlag, Stuttgart.
- Rao, C.R. (1973): *Linear Statistical Inference and Its Applications*. Second Edition, John Wiley & Sons, New York.
- Remondi, B.W. (1984): "Using the Global Positioning System (GPS) Phase Observable for Relative Geodesy: Modeling, Processing and Results." Ph.D. Dissertation, Centre for Space Research, The University of Texas at Austin, Austin, Texas.
- Remondi, B.W. (1990): "Recent Advances in Pseudo-Kinematic GPS." Proceedings of the Second International Symposium on Precise Positioning with the Global Positioning System, Ottawa, Canada, Sept. 1990.
- Salzmann, M.A. and P.J.G., Teunissen (1989): "Quality Control in Kinematic Data Processing." Presented at the second international symposium on land vehicle navigation, Munster, Germany.
- Schwarz, K.P., M.E., Cannon and R.V.C., Wong (1989): "A comparison of GPS kinematic models for the determination of position and velocity along a trajectory." *manuscripta geodaetica*, Vol. 14, No. 5, pp. 345-353.

- Seeber, G., A., Schuchardt and G., Wubben (1986): " Precise Positioning Results with TI4100 GPS Receivers on Moving Platforms." Proc. of the Fourth International Geodetic Symposium on Satellite Positioning, Austin, Texas.
- Teunissen, P.J.G. and Salzmann, M.A. (1989): "A recursive slippage test for use in state-space filtering." *manuscripta geodaetica*, Vol. 14, pp 383-390.
- Teunissen, P.J.G. (1990): " Quality control in integrated navigation systems." Proc. IEEE PLANS'90, Las Vegas, U.S.A.
- Wei, M., D. Lapucha and H. Martell (1990): " Fault Detection and Estimation in Dynamic Systems." Proceedings of IAG International Symposium 107 on Kinematic Systems in Geodesy, Surveying and Remote Sensing, Springer Verlag, New York.
- Wells, D.E., N. Beck, D. Delikaraoglu, A. Kleusberg, E.J. Krakiwsky, G., Lachapelle, R.B. Langley, M. Nakiboglu, K.P. Schwarz, J.M. Tranquilla, P. Vanicek (1986): *Guide to GPS Positioning*. Canadian GPS Associates, Fredericton, New Brunswick, Canada.
- Willsky, A. S. (1976): "A Survey of Design Methods for Failure Detection in Dynamic Systems." *Automatica*, Vol. 12, pp. 601-611.
- Wubben, G. (1989): " The GPS Adjustment Software Package GEONAP: Concepts and Models." Proceedings of the 5th International Geodetic Symposium on Satellite Positioning, New Mexico State University, Las Cruces, N.M. Vol.2 pp. 452-461